Ocean Engineering 233 (2021) 109084

Contents lists available at ScienceDirect

Ocean Engineering

journal homepage: www.elsevier.com/locate/oceaneng

Tuning of vessel parameters including sea state dependent roll damping

Xu Han *, Svein Sævik, Bernt Johan Leira

Department of Marine Technology, Norwegian University of Science and Technology (NTNU), 7491 Trondheim, Norway
Centre for Research-based Innovation on Marine Operations (SFI MOVE), Norway

ARTICLE INFO

Keywords:
Online model tuning
Discrete Bayesian updating
Roll damping
Gaussian process regression
Stochastic Kriging
Wave-induced vessel motion

ABSTRACT

Online tuning of vessel models based on onboard measurement data can reduce the uncertainties of vessel motion prediction, and therefore potentially increase the safety and cost efficiency for marine operations. Among the uncertain vessel parameters, the roll damping coefficient is very important and highly nonlinear. In reality, roll damping depends on the sea state and vessel condition. This paper proposes two different procedures for tuning the sea state dependent roll damping coefficient together with other uncertain vessel parameters, i.e., 1-step tuning and 2-step tuning procedures. In addition, a roll damping prediction model based on Gaussian process regression is also proposed to predict the roll damping for future sea states based on historical data. The tuning procedure together with the proposed prediction model form an iterative closed loop of continuously improving the knowledge about the roll damping online, also estimating the model uncertainty based on prior knowledge, sampling uncertainties, and the applied kernel. Case studies are presented to demonstrate the procedures.

1. Introduction

Reliable vessel motion prediction plays a key role for the safety and optimization of maritime and offshore activities. Among the vessel motions induced by different environmental sources, the wave-frequent ones can be most critical to predict because they are most difficult to control. In engineering practice, it is acceptable to simplify the relation between wave elevation and the rigid body vessel motions by linearization of the transfer functions in the frequency domain, especially for typical marine operations executed at moderate seas (DNVGL-ST-N001, 2016). The vessel motion linear transfer functions for the 6 degrees of freedom (DOFs) in complex form are usually also referred to as Response Amplitude Operators (RAOs). The roll motion is widely recognized as the most critical and challenging response quantity to predict, because the critical roll motion near resonance is extremely influenced by the estimated damping which is significantly underpredicted by the linear potential theory.

Roll damping is highly nonlinear and has therefore attracted huge research interest for more than a century (Falzarano et al., 2015). System modelling usually requires simplifications which result in model uncertainties and errors. Linearization of roll damping is common practice for seakeeping analysis in order to estimate the linear transfer function between wave elevation and vessel roll motion, i.e., the roll RAO. For irregular waves, the roll damping is linearized by minimizing the error between the linearized and the real system with the assumption that both input to and output from the system are Gaussian processes (Kaplan, 1966). This is called stochastic linearization.

The Watanabe–Inoue–Takahashi formula may be applied to estimate the total roll damping for varying u (vessel forward speed), ϕ_A (roll amplitude), ω (wave frequency), and ship forms (Himeno, 1981). However, the estimation seems only acceptable for normally loaded ships near their natural frequencies (Himeno, 1981). A third-order polynomial formula may well model the nonlinearity between the non-dimensional equivalent linear roll damping ($\hat{B}_{44}$) and the non-dimensional frequency ($\hat{\omega}$) for each combination of u, ϕ_A, vessel loading, and ship form based on Tasai–Takaki's Table reported in English by Himeno (1981). However, the $\hat{B}_{44}$ as a function of e.g., ship form and speed is not clear.

About half a century ago, Ikeda, Himeno, Tanaka, and their teams from Osaka Prefecture University heavily contributed to understanding and modelling the nonlinear roll damping in a systematic manner. Their work of separating the roll damping into several components and ignoring their interactions recommended by ITTC (2011), basically forms the present engineering practice of ship roll damping estimation in the absence of experimental data. Known as Ikeda's method, the equivalent linear roll damping B_{44} can be separated as follows Himeno (1981)

$$B_{44} = B_W + B_F + B_E + B_L + B_{BK} \tag{1}$$

* Corresponding author at: Department of Marine Technology, Norwegian University of Science and Technology (NTNU), 7491 Trondheim, Norway.
E-mail address: xu.han@ntnu.no (X. Han).

https://doi.org/10.1016/j.oceaneng.2021.109084
Received 29 September 2020; Received in revised form 14 April 2021; Accepted 24 April 2021
Available online 1 June 2021

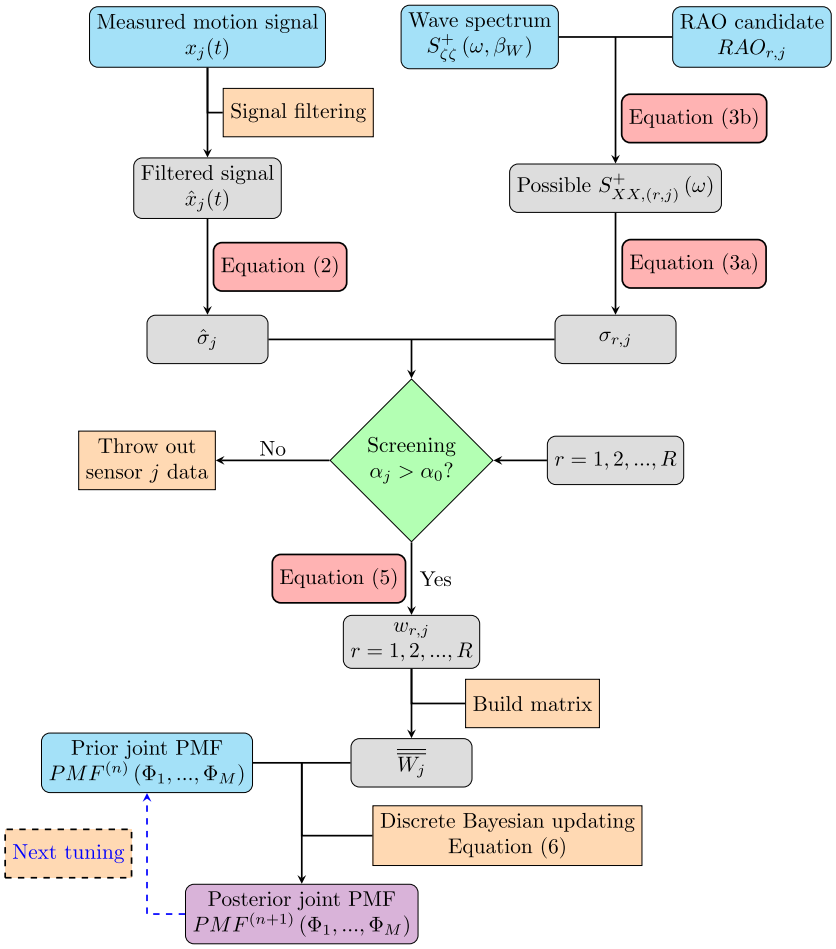

Fig. 1. Process of tuning vessel model parameters, based on the vessel motion signal $x_j(t)$ and the wave spectrum. Precise knowledge about the wave spectrum is assumed.

where B_W is the wave damping, B_F is the friction damping caused by hull skin-friction, B_E is the damping due to eddy making, B_L is the linear lift damping, B_{BK} is the damping due to the bilge keels. Among them, B_W and B_L are linearly proportional to roll angular velocity, while the other components are nonlinear. B_F is relatively less important and may be neglected for full scale ships (Himeno, 1981). Ikeda et al. (1978a,b,c, 1979) proposed formulas for estimating most of the important roll damping components by a semi-empirical approach. Even though Ikeda's formulas are recommended by ITTC (2011), cautions should be taken, because (1) Ikeda's formulas are limited to certain ship forms; and (2) Ikeda's formulas were derived for pure roll motion based on still water condition (Larsen et al., 2019). For example, the use of panel methods to predict the wave damping (B_W) with forward speed is theoretically accurate and recommended (Falzarano et al., 2015) over the semi-empirical Ikeda's formulas (Ikeda et al., 1978b). Söder et al. (2017) found that the Ikeda's formulas significantly overestimated the hull lift damping component while underestimating the bilge keel damping by benchmarking with model test data.

Consequently, model tests or empirical data are always preferred for new vessel design in order to model the roll damping with sufficient accuracy. Free decay model tests are normally performed to obtain the roll damping, however, only at the important damped roll resonance frequency. Forced rolling model tests can be performed to obtain the roll damping at other frequencies. However, this is frequently not performed. In addition, much more model tests are required if the roll amplitude dependent damping coefficients are wanted. By fitting to the empirical data, the total roll damping can be modelled as functions of vessel speed u, vessel draught D, roll amplitude ϕ_A (or wave amplitude A), wave frequency ω, etc.

However, the scale effects of model tests may significantly affect the accuracy of the roll damping estimation (Söder and Rosén, 2015). At present, prediction of roll damping based on numerical simulation by computational fluid dynamics (CFD) codes has also received considerable attention, e.g., Irkal et al. (2016). However, a reliable CFD analysis requires high competence in modelling and understanding the limitations of the codes and the applied algorithms. Usually, results from CFD analyses require validation from model tests. Both model tests and high-fidelity analyses are expensive and time-consuming. Therefore, it is of great interest to improve the knowledge of the roll damping for the specific vessel throughout its whole life cycle by using the weather information and the vessel motion measurements onboard. In practice, the additional damping can be considered as a function of parameters related to the sea state and vessel condition, i.e., $B_{44} = f(\boldsymbol{x})$ where $\boldsymbol{x} = [u, D, H_s, T_p, \beta_W, \dots]$, H_s is the significant wave height, T_p is the spectral wave peak period, β_W is the wave direction. With such a roll damping function, the RAO and roll motions can be estimated at a specific wave and vessel condition by assuming stationarity. Consequently the improved roll damping model built upon on-site measurements can potentially increase the cost efficiency and safety for marine operations.

It is very challenging to update the roll damping by on-site measurements and weather information, because (1) measurements and weather information are subject to significant uncertainties (Bitner-Gregersen and Hagen, 1990; Qiu et al., 2014); and (2) there are also many other vessel parameters subject to uncertainties, e.g., inertia items (Han et al., 2020). Therefore, all the uncertain parameters should

be identified first and tuned simultaneously in a probabilistic way. An earlier case study by Han et al. (2020) indicates that multiple sensors at different locations providing signals of displacements, velocities, and accelerations can help identifying the uncertain vessel parameters. Han et al. (2021a) proposed an algorithm for tuning of vessel model parameters by Bayesian inference. Tuning of the uncertain vessel parameters in a probabilistic approach can improve the knowledge about the real-time vessel condition and reduce the model uncertainties quantitatively, based on onboard vessel motion measurements and wave information such as H_s, T_p, β_W, directional spreading, and spectral shape.

Vessel parameters can be sea state dependent, vessel condition dependent, or permanent (Han et al., 2020). The sea state dependent parameters (e.g., roll damping) usually also depend on vessel conditions (e.g., loading conditions and vessel forward speed). Han et al. (2021a) considered a constant roll damping coefficient through different sea states for tuning, and pointed out that the algorithm should be further developed to tune vessel roll damping as being sea state dependent. The present paper describes the algorithm for tuning of sea state dependent roll damping coefficient together with other vessel parameters. In addition, it is even more important for this paper to establish an algorithm which prescribes how to model the roll damping as sea state dependent and predict it for the unobserved future sea states. This is considered particularly challenging because:

1. The tuned roll damping value is only valid for the current sea state, which does not directly help predicting the vessel roll damping for other sea states. Therefore, the algorithm should be able to predict the roll damping for the unobserved sea states with improved accuracy based on prior knowledge and historical tuning results for different sea states and vessel conditions.
2. As discussed previously, it is difficult to define a function in advance that is sufficiently accurate for modelling of roll damping.
3. The number of available full-scale measurements can be very limited and insufficient. Under-fitting or over-fitting can be expected.
4. The available measurements may also be concentrated around certain sea states. It is questionable to predict roll damping for other sea states by extrapolation based on any fitted curve.

The paper is organized as follows. The basic vessel model tuning algorithm is described in Section 2 (Han et al., 2021a). For flexible modelling of roll damping, Gaussian process regression is introduced in Section 3. In Section 4, two procedures are proposed to modify the basic model tuning algorithm in order to tune and represent roll damping as being sea state dependent. Numerical case studies are carried out to demonstrate the performance of the proposed tuning procedures and the corresponding roll damping prediction model. The basis of the case studies are described in Section 5, and the results are shown in Section 6. Finally, Section 7 concludes and discusses the findings, limitations, and future work related to the present research.

2. Basic vessel model tuning procedure

The applied algorithm for tuning of vessel seakeeping parameters based on wave information and vessel motion measurements proposed by Han et al. (2021a) is briefly repeated here for completeness purposes. The algorithm is also illustrated in Fig. 1.

Firstly, the uncertain vessel parameters (i.e., $\boldsymbol{\Phi}_1, \boldsymbol{\Phi}_2, \ldots, \boldsymbol{\Phi}_m, \ldots, \boldsymbol{\Phi}_M$, $m \in \{1, 2, \ldots, M\}$) are identified based on their sensitivities with respect to the measured vessel motions of primary interest. This can be achieved by performing uncertainty and sensitivity analyses, e.g., Han et al. (2020). The uncertainty ranges of those parameters can be determined based on the relevant prior information such as available design and analysis documentation, accuracy of onboard monitoring data, and engineering judgement. Each uncertain parameter $\boldsymbol{\Phi}_m$ is then discretized evenly into Im values within its uncertainty range. For a successful tuning, it is important to have a sufficiently large uncertainty range for each $\boldsymbol{\Phi}_m$ while the spacing between the discretized values should be sufficiently small to capture any critical nonlinear behaviour. Considering reasonable uncertainty ranges based on practical prior information, 5 to 8 discrete values for each vessel parameter can be sufficient for the tuning. Combining the uncertain parameters at their discrete values, a total number of $R = I1 \times I2 \times \cdots \times IM$ discrete assessment points are defined, for calculating the possible RAOs. In addition, multiple quantities of vessel motions (e.g., displacement, velocity, and acceleration for different DOFs at different locations) are normally required for the tuning process. Each of the considered measured vessel motion quantities is indexed by $j \in \{1, 2, \ldots, J\}$. Consequently, a RAO database containing $R \times J$ RAOs can be established by performing seakeeping analysis for those measured quantities at those discrete combinations of the uncertain parameters.

The joint probability distribution of the identified uncertain vessel parameters is denoted as $P^{(n)}\left(\boldsymbol{\Phi}_1, \boldsymbol{\Phi}_2, \ldots, \boldsymbol{\Phi}_M\right)$. The superscript n stands for the number of completed iterative updates based on the proposed tuning procedure. The joint probability distribution is tuned for each stationary wave and vessel condition. Typically, for a vessel in steady condition with respect to heading, advancing speed, and inertia distribution, the stationarity is determined by the duration of a stationary sea state which could vary from 20 min to 3 hr, depending on geometrical location. With the information on waves (e.g., a wave spectrum), vessel motion measurements (e.g., signal $x_j(t)$ for the measured quantity j), and a RAO database covering the uncertainty ranges of the uncertain vessel parameters, the tuning can be performed as follows:

1. Filter the vessel motion measurements $x_j(t)$ to obtain the vessel motion time series in the wave frequency domain. The high-frequency components (e.g., signal noise) and the low-frequency components (e.g., signal bias, second-order motions) are important to be filtered out. The filtered signal is denoted as $\hat{x}_j(t)$
2. Calculate the standard deviation of the filtered signal, $\hat{\sigma}_j$, by

$$\hat{\sigma}_j = \sqrt{\frac{\sum_{t=1}^{N_t}\left(\hat{x}_j(t) - \bar{x}_j\right)^2}{\left(N_t - 1\right)}} \tag{2a}$$

$$\bar{x}_j = \frac{\sum_{t=1}^{N_t}\hat{x}_j(t)}{N_t} \tag{2b}$$

where N_t is the total number of time steps of the signal, and $\bar{x}_j$ is the mean value of the filtered signal. The duration of the signal $x_j(t)$, $T = N_t \Delta t$ (where Δt is the time interval), should be selected such that the sea state and vessel condition remains stationary within the duration of T, while the sampling variability should be sufficiently small. A typical value of T can be 20 min to 1 hr.

3. Calculate the standard deviations of the possible vessel response $\sigma_{r,j}$, based on the wave spectrum and the candidate RAO from the RAO database for the measured quantity j (i.e., $RAO_{r,j}$)

$$\sigma_{r,j} = \sqrt{\sum_{n=1}^{N_\omega} S^+_{XX,(r,j)}\left(\omega_n\right) \cdot \Delta\omega} \tag{3a}$$

$$S^+_{XX,(r,j)}(\omega) = \left|H_{r,j}\left(\omega, \beta_W\right)\right|^2 \cdot S^+_{\zeta\zeta}\left(\omega, \beta_W\right) \tag{3b}$$

where N_ω is the total number of the discretized frequencies for the response spectrum, $S^+_{\zeta\zeta}\left(\omega, \beta_W\right)$ is the long-crested wave spectrum, and S^+ stands for a single-sided power spectrum. $S^+_{XX,(r,j)}(\omega)$ is the possible response spectrum for the response X corresponding to the measured quantity j based on the vessel parameter combination r, $H_{r,j}\left(\omega, \beta_W\right)$ is the corresponding linear transfer function (i.e., $RAO_{r,j}$) between wave elevation and vessel response. Each possible combination of the considered vessel parameters, i.e., $\left(\phi_{i1}, \phi_{i2}, \ldots, \phi_{iM}\right)$, is subscripted with

number $r \in \{1,2,\dots,R\}$, where ϕ_{im} for $m \in \{1,2,\dots,M\}$ is the imth discrete value of the considered uncertain vessel parameter Φ_m in the RAO database. $R = \prod_{m=1}^{M}(Im)$, is the total number of vessel parameter combinations and Im is the number of the discretized values of Φ_m in the RAO database. For all possible vessel parameter combinations, $\sigma_{r,j}$ should be calculated.

4. Less sensitive measured quantities for the considered uncertain vessel parameters at the current sea state $S^{+}_{\zeta\zeta}(\omega,\beta_W)$ should be screened out. The sensor screening ratio (SSR) α_j is introduced to quantify the importance of the measured quantity j

$$\alpha_j = \frac{\sigma_{\sigma_{r,j}}}{\hat{\sigma}_j} \tag{4a}$$

$$\sigma_{\sigma_{r,j}} = \sqrt{\frac{\sum_{r=1}^{R}\left(\sigma_{r,j}-\bar{\sigma}_{R,j}\right)^2}{R-1}} \tag{4b}$$

$$\bar{\sigma}_{R,j} = \frac{\sum_{r=1}^{R}\sigma_{r,j}}{R} \tag{4c}$$

where $\sigma_{\sigma_{r,j}}$ is the standard deviation of $\sigma_{r,j}$ over $r = 1,2,\dots,R$. The case study uses a screening criterion of $\alpha_0 = 0.05$. If $\alpha_j < \alpha_0$, the signal of the quantity j will be excluded during the process of tuning the parameters. SSR basically represents the importance of the obtained measurements for tuning of the considered vessel parameters for the present sea state. The selection of the criterion value α_0 depends on the uncertainties of the measurements and the system errors introduced by application of linear potential theory to represent the true vessel dynamics within the wave frequency band. The influence of the introduced screening criterion on the final tuning results is discussed by detailed sensitivity studies in Han et al. (2021a).

5. Calculate the weight factor for each parameter combination r by inverse distance weighting (Shepard, 1968)

$$w_{r,j} = \frac{1}{\left|\sigma_{r,j}-\hat{\sigma}_j\right|^p} \tag{5}$$

where $p \in \mathbb{R}^+$ is called the power parameter. The choice of the p value depends on the number of considered uncertain parameters, their sensitivity and uncertainty ranges, and engineering judgements. The influence of the p value on the tuning results was studied by Han et al. (2021a).

6. Build the likelihood function for updating the joint probability distribution of the considered uncertain parameters ($\Phi_1, \Phi_2, \dots, \Phi_M$). First, establish the weight matrix $\overline{\overline{W_j}}$ for all $r \in \{1,2,\dots,R\}$ in the RAO database. The weight matrix would have M dimensions with the size of $I1 \times I2 \times \cdots \times IM$. Then linearly interpolate the weight matrix $\overline{\overline{W_j}}$ from the size of $I1\times I2\times\cdots\times IM$ (variable resolution in the RAO database) to the size of $K1 \times K2\times\cdots\times KM$ (variable resolution in the discrete joint probability distribution).

7. Update the joint probability distribution $P^{(n+1)}(\Phi_1,\Phi_2,\dots,\Phi_M)$. Since the likelihood function (i.e., weight matrix $\overline{\overline{W_j}}$) is presented at limited number of parameter combinations, $r \in \{1,2,\dots,N_{Prob}\}$, where $N_{Prob} = \prod_{m=1}^{M}(Km)$ and Km is the number of the discretized values of Φ_m in the discrete joint probability distribution, updating the joint probability distribution based on discrete Bayesian inference (Labbe, 2018) must therefore be calculated at those discretized points, i.e.,

$$PMF^{(n+1)}(\Phi_1,\dots,\Phi_M) = \mathcal{NO}\left(PMF^{(n)}(\Phi_1,\dots,\Phi_M)\odot\overline{\overline{W_j}}\right) \tag{6}$$

where PMF means the joint probability mass function, $\odot$ operator means the element-wise multiplication of the two matrices of the same dimension, i.e., a Hadamard product (Scheick, 1997).

To ensure that the sum of the joint probability mass function remains 1.0, normalization $\mathcal{NO}(\cdot)$ is required. Physically, the uncertain vessel parameters are continuous variables. Therefore, the joint probability density function (PDF) is more appropriate to represent their uncertainties. Numerically, the relation between joint PMF and joint PDF can be approximated by:

$$PMF(\phi_{k1},\phi_{k2},\dots,\phi_{kM}) = PDF(\phi_{k1},\phi_{k2},\dots,\phi_{kM})\prod_{m=1}^{M}\Delta\Phi_m \tag{7}$$

where ϕ_{km} for $m \in \{1,2,\dots,M\}$ is the kmth discrete value for the variable Φ_m, $\Delta\Phi_m$ is the interval between the discrete values of variable Φ_m.

The algorithm applies statistical inference of the direction-independent vessel parameters based on onboard measurements and wave information. Consequently, the tuned vessel model can be applied to predict the vessel motion for other sea states and wave directions, with quantified parameter uncertainties.

3. GaussIan process regression

Gaussian process regression (GPR) is found to be a very promising solution for roll damping modelling and prediction, because (1) it does not require to decide the format of the roll damping function; (2) the tuned values of roll damping for the previous sea states and vessel conditions can reasonably influence the prediction of roll damping for future sea states and vessel conditions, through the covariance function; (3) it also indicates the estimation uncertainty based on the prior knowledge, the available samples, and the selected kernel function.

GPR is fundamentally based on the conditional distribution of multivariate Gaussian vectors (Rasmussen and Williams, 2006). For a $N+M$ dimensional multivariate Gaussian vector $\boldsymbol{y}$

$$\boldsymbol{y} = \begin{bmatrix}\boldsymbol{y}_1\\ \boldsymbol{y}_2\end{bmatrix} \left(\text{with sizes } \begin{bmatrix}N\times 1\\ M\times 1\end{bmatrix}\right) \tag{8}$$

where $\mathbf{y}_1$ and $\mathbf{y}_2$ are also multivariate Gaussian vectors and the mean vector $\boldsymbol{\mu}$ and the covariance matrix $\boldsymbol{\Sigma}$ can be written as

$$\boldsymbol{\mu} = \begin{bmatrix}\boldsymbol{\mu}_1\\ \boldsymbol{\mu}_2\end{bmatrix} \left(\text{with sizes } \begin{bmatrix}N\times 1\\ M\times 1\end{bmatrix}\right) \tag{9a}$$

$$\boldsymbol{\Sigma} = \begin{bmatrix}\boldsymbol{\Sigma}_{11} & \boldsymbol{\Sigma}_{12}\\ \boldsymbol{\Sigma}_{21} & \boldsymbol{\Sigma}_{22}\end{bmatrix} \left(\text{with sizes } \begin{bmatrix}N\times N & N\times M\\ M\times N & M\times M\end{bmatrix}\right) \tag{9b}$$

then the conditional distribution of $\boldsymbol{y}_2$ on $\boldsymbol{y}_1 = \tilde{\boldsymbol{y}}_1$ is also a multivariate Gaussian distribution, i.e.,

$$(\boldsymbol{y}_2|\boldsymbol{y}_1 = \tilde{\boldsymbol{y}}_1) \sim \mathcal{N}(\bar{\boldsymbol{\mu}}_2, \bar{\boldsymbol{\Sigma}}_{22}) \tag{10a}$$

$$\bar{\boldsymbol{\mu}}_2 = \boldsymbol{\mu}_2 + \boldsymbol{\Sigma}_{21}\boldsymbol{\Sigma}_{11}^{-1}(\tilde{\boldsymbol{y}}_1 - \boldsymbol{\mu}_1) \tag{10b}$$

$$\bar{\boldsymbol{\Sigma}}_{22} = \boldsymbol{\Sigma}_{22} - \boldsymbol{\Sigma}_{21}\boldsymbol{\Sigma}_{11}^{-1}\boldsymbol{\Sigma}_{12} \tag{10c}$$

This means that the distribution of $\boldsymbol{y}_2$ can be updated based on the known samples $\boldsymbol{y}_1 = \tilde{\boldsymbol{y}}_1$ and the covariance matrix for $\boldsymbol{y}_2$ and $\boldsymbol{y}_1$. It is worth noting that updating of the variance matrix $\boldsymbol{\Sigma}_{22}$, i.e., Eq. (10c), does not rely on the observed values of $\boldsymbol{y}_1$, i.e., $\tilde{\boldsymbol{y}}_1$.

For a continuous function $y = f(x)$, each y value (i.e. $y_i = f(x_i)$, $i \in \mathbb{Z}^+$) can be considered as a Gaussian distributed random variable, i.e., $y_i \sim \mathcal{N}(\mu_i, \sigma_i)$, and all variables are correlated. By having samples at some known points $\boldsymbol{x}_1$ (i.e., $\boldsymbol{y}_1 = f(\boldsymbol{x}_1) = \tilde{\boldsymbol{y}}_1$), the corresponding predictions at other points (e.g., $\boldsymbol{y}_2 = f(\boldsymbol{x}_2)$) can be estimated based on Eqs. (9) and (10) if the covariance matrix of the variables for $\boldsymbol{y}_1$ and $\boldsymbol{y}_2$ (i.e., $\boldsymbol{\Sigma}$) can be established.

The covariance matrix is called the kernel or the similarity function, which establishes the correlation among data points. It is physically reasonable to consider the kernel (covariance coefficient) $K(x_i, x_j) = cov(i,j)$ between $y_i = f(x_i)$ and $y_j = f(x_j)$ to be a function of the distance along the input axis (i.e. $K(x_i, x_j) = g(|x_i - x_j|)$). Among

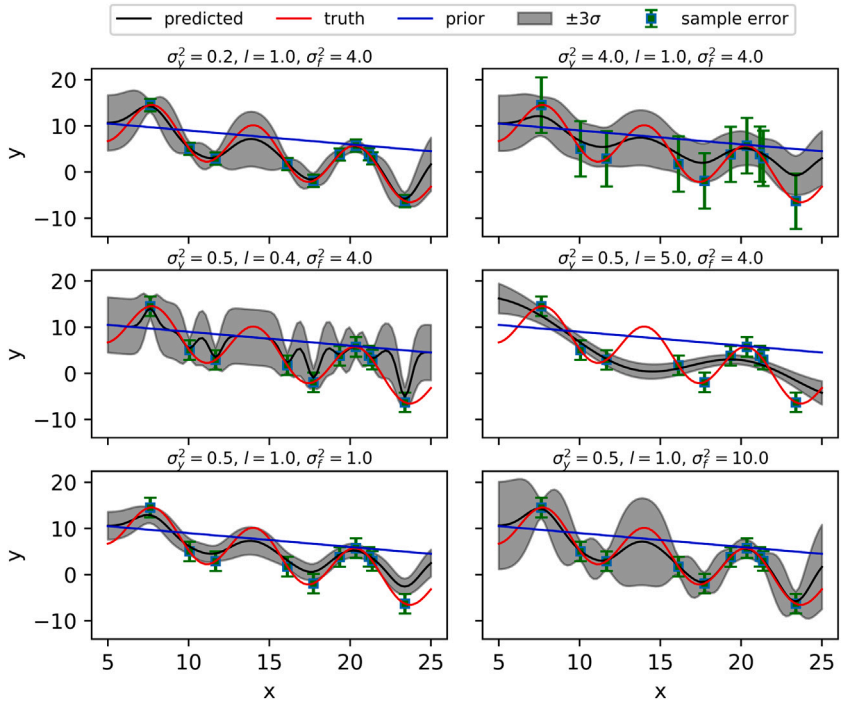

Fig. 2. The influence of GPR hyperparameters on the prediction curve.

many kernel designs, the radial-basis function (RBF) is the most popular kernel, i.e.,

$$K(x_i, x_j) = \sigma_f^2 \exp(-\frac{1}{2l^2}(x_i - x_j)^2) \tag{11}$$

where two hyperparameters are introduced. σ_f^2 is called signal variance which represents the prior knowledge about the variance of the random process. l is called length-scale.

In reality, samples are also subject to uncertainties. In the input space $\boldsymbol{Y}$, the observed samples $\tilde{\boldsymbol{Y}}$ can be written as

$$\tilde{\boldsymbol{Y}} = f(\boldsymbol{X}) + \boldsymbol{\epsilon} \tag{12}$$

where the $\boldsymbol{\epsilon}$ vector represents the uncertainties for the samples. For each sample $\tilde{y}_i$, the uncertainty ϵ_i is also considered to be a Gaussian variable:

$$\epsilon_i \sim \mathcal{N}(0, \sigma_{y_i}^2) \tag{13}$$

where $\sigma_{y_i}^2$ represents the uncertainty level for the observed sample y_i. Consequently, for predicting $\boldsymbol{y}_* = f(\boldsymbol{x}_*)$, Eq. (10) can be modified to account for sampling noise:

$$(\boldsymbol{y}_*|\boldsymbol{Y} = \tilde{\boldsymbol{Y}}) \sim \mathcal{N}(\bar{\boldsymbol{\mu}}_*, \bar{\boldsymbol{K}}_{**}) \tag{14a}$$

$$\bar{\boldsymbol{\mu}}_* = \boldsymbol{\mu}_* + \boldsymbol{K}_{*Y}\boldsymbol{K}_{\tilde{Y}}^{-1}(\tilde{\boldsymbol{Y}} - \boldsymbol{\mu}_Y) \tag{14b}$$

$$\bar{\boldsymbol{K}}_{**} = \boldsymbol{K}_{**} - \boldsymbol{K}_{*Y}\boldsymbol{K}_{\tilde{Y}}^{-1}\boldsymbol{K}_{Y*} \tag{14c}$$

where $\boldsymbol{Y}$ is the input space, $\tilde{\boldsymbol{Y}}$ is the observed samples for the input space, $\boldsymbol{y}_*$ is the space to be predicted (prediction space). $\bar{\boldsymbol{\mu}}_*$ and $\bar{\boldsymbol{K}}_{**}$ are the conditional mean and the updated kernel (i.e., the similarity function) for the prediction space. $\boldsymbol{\mu}_*$ and $\boldsymbol{\mu}_Y$ represent the prior means. $\boldsymbol{K}_{*Y}$ and $\boldsymbol{K}_{Y*}$ are the kernels representing the correlations between the input space and the prediction space, calculated based on Eq. (11). $\boldsymbol{K}_{\tilde{Y}}$ can be calculated by

$$\boldsymbol{K}_{\tilde{Y}} = \boldsymbol{K}_Y + \boldsymbol{\Sigma}_Y \tag{15a}$$

$$\boldsymbol{K}_Y = \begin{bmatrix} K(x_1,x_1) & \dots & K(x_1,x_j) & \dots & K(x_1,x_N) \\ & \ddots & & & \vdots \\ & & K(x_i,x_j) & \dots & K(x_i,x_N) \\ & & & \ddots & \vdots \\ & & & & K(x_N,x_N) \end{bmatrix} \tag{15b}$$

$$\boldsymbol{\Sigma}_Y = \begin{bmatrix} \sigma_{y1}^2 & & & & \\ & \ddots & & & \\ & & \sigma_{yi}^2 & & \\ & & & \ddots & \\ & & & & \sigma_{yN}^2 \end{bmatrix} \tag{15c}$$

where $\boldsymbol{K}_Y$ is the kernel for the input space with each element calculated based on Eq. (11). $\boldsymbol{\Sigma}_Y$ is a $N \times N$ diagonal matrix. Note that $\boldsymbol{K}_{\tilde{Y}}$ is no longer the covariance matrix for the input space, because it includes the uncertainties of the observations. Eqs. (14) and (15) including the sampling uncertainties is called stochastic Kriging.

GPR is a "non-parametric" method, meaning that the regression does not require knowing the form or the order of the function. GPR is sometimes also considered as an "infinite-parametric" method, because it ideally requires infinite samples in order to perfectly model the function.

Fig. 2, as an example, illustrates how the GPR hyperparameters influence the prediction. Larger σ_y^2 helps to smoothen the fitted curve/surface. For the sample with uncertainties, σ_y^2 represents its sample uncertainty/error. The length-scale l indicates how strong the correlation is between the points in that dimension. In addition to σ_y^2, the length-scale may also help the regression avoiding over-fitting and under-fitting. σ_f^2 represents the variance of the prior knowledge about the model. It can be interpreted as the variance of a point that is far away from all the available sample points (i.e., negligible correlation).

The stochastic Kriging algorithm (Rasmussen and Williams, 2006) as implemented in the Python package scikit-learn (sklearn hereafter) (Pedregosa et al., 2011) has been used. The GPR in sklearn has been demonstrated as "near the best" GPR programme with respect to its analysis performance and computational speed (Erickson et al., 2018). The GPR model in sklearn assumes zero prior mean. It is practically acceptable since the GPR model converges according to the available samples and independent of the provided prior mean if the amount of training data is sufficiently large. However, to ensure accuracy for research purpose, non-zero prior mean is considered in the study. Based on the fact that the prior mean vector does not influence the covariance matrix for the multivariate Gaussian distribution, i.e.,

$$\begin{bmatrix} \boldsymbol{Y} \\ \boldsymbol{y}_* \end{bmatrix} \sim \mathcal{N}\left(\begin{bmatrix} \boldsymbol{\mu}_Y \\ \boldsymbol{\mu}_* \end{bmatrix}, \begin{bmatrix} \boldsymbol{K}_{\tilde{Y}} & \boldsymbol{K}_{Y*} \\ \boldsymbol{K}_{*Y} & \boldsymbol{K}_{**} \end{bmatrix}\right) \text{ is equivalent to,}$$

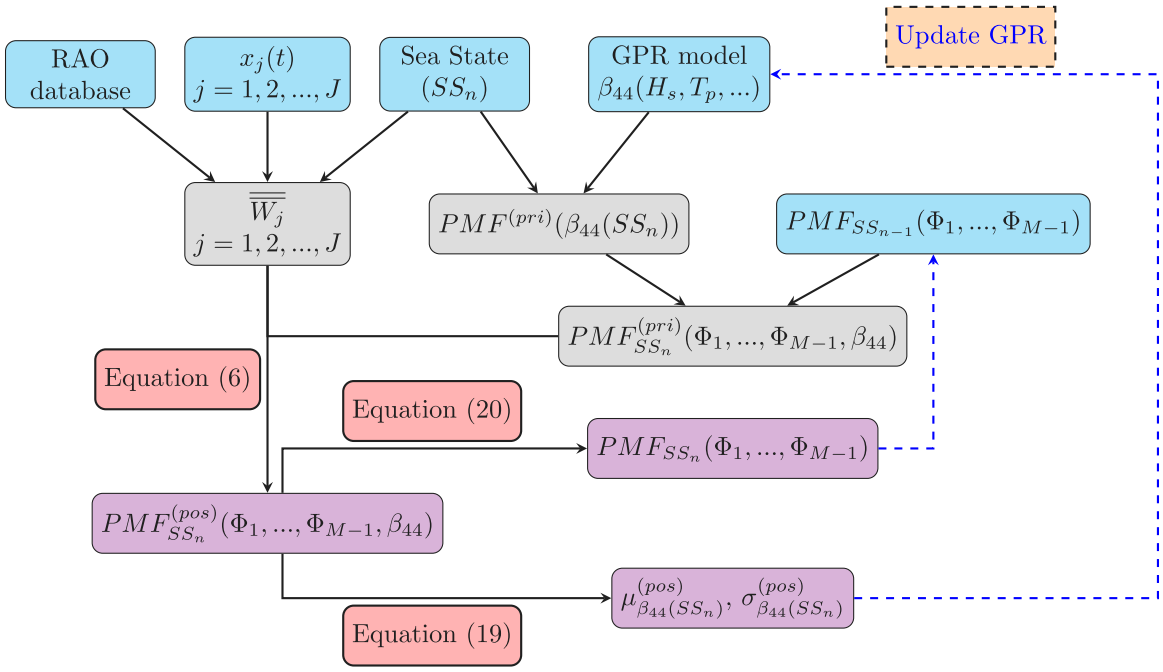

Fig. 3. Process of the 1-step tuning of vessel parameters including sea state dependent β_{44} and updating the β_{44} GPR model, assuming $\boldsymbol{\Phi}_M = \beta_{44}$.

$$\begin{bmatrix} \boldsymbol{Y} - \boldsymbol{\mu}_{\boldsymbol{Y}} \\ \boldsymbol{y}_* - \boldsymbol{\mu}_* \end{bmatrix} \sim \mathcal{N}\left(\begin{bmatrix} \boldsymbol{0} \\ \boldsymbol{0} \end{bmatrix}, \begin{bmatrix} \boldsymbol{K}_{\tilde{Y}} & \boldsymbol{K}_{Y*} \\ \boldsymbol{K}_{*Y} & \boldsymbol{K}_{**} \end{bmatrix} \right) \tag{16}$$

The prior mean will accordingly be subtracted from the values at the data points before the GPR model fitting, whereas it will be added to the predicted value for the prediction based on the fitted GPR model.

Tuning the hyperparameters may be based on personal experience and engineering judgement. However, these hyperparameters can also be automatically optimized, by assuming that the input data points ($\tilde{\boldsymbol{Y}}$) are given at their maximum likelihood. The log marginal likelihood for a zero mean prior can be written as (Rasmussen and Williams, 2006)

$$\log p(\tilde{\boldsymbol{Y}}|\boldsymbol{X}) = \log \mathcal{N}(\tilde{\boldsymbol{Y}}|\boldsymbol{0}, \boldsymbol{K}_{\tilde{Y}}) = -\frac{1}{2}\tilde{\boldsymbol{Y}}^T \boldsymbol{K}_{\tilde{Y}}^{-1}\tilde{\boldsymbol{Y}} - -\frac{1}{2}\log|\boldsymbol{K}_{\tilde{Y}}| - \frac{N}{2}\log(2\pi) \tag{17}$$

where N is the number of samples. In order to better control the GPR model for the present research, the hyperparameters of the kernel are manually determined without applying the sampling dependent optimization in Eq. (17).

4. Proposed procedure for tuning of vessel parameters including sea state dependent roll damping

4.1. One-step tuning procedure

In order to interactively tune sea state dependent roll damping and improve the roll damping prediction model (i.e., the GPR model), the model tuning algorithm described in Section 2 is modified, as illustrated in Fig. 3. Assume that the joint probability distribution of the uncertain vessel parameters have been tuned for $n-1$ sea states (and so as to the GPR model of β_{44}). The procedure of tuning vessel parameters and updating the GPR model based on the measurements (i.e., $x_j(t)$, $j = 1, 2, \ldots, J$) and the corresponding wave information for the next sea state SS_n is described below. $SS_n \in \mathbb{Z}^+$, is the index of the sea state (i.e., sea state number).

1. Given the wave information for the sea state SS_n and the updated GPR model from previous sea states, the additional roll damping coefficient β_{44} can be predicted, in terms of its mean and variance values. Then the probability mass function of $\beta_{44}(SS_n)$ can be established at the discrete values, assuming it is Gaussian distributed.
2. Together with the available knowledge about other uncertain vessel parameters after the previous sea state SS_{n-1}, i.e., $PMF_{SS_{n-1}}(\boldsymbol{\Phi}_1, \ldots, \boldsymbol{\Phi}_{M-1})$, the joint probability distribution including β_{44} can be calculated by multiplying the probability mass functions of $\beta_{44}(SS_n)$ and the other parameters at their discrete values, i.e.,

$$PMF^{(pri)}_{SS_n}(\phi_{k1}, \ldots, \phi_{k(M-1)}, \phi_{kM}) = PMF_{SS_{n-1}}(\phi_{k1}, \phi_{k2}, \ldots, \phi_{k(M-1)}) \cdot PMF(\phi_{kM}(SS_n)) \tag{18}$$

where ϕ_{km} for $m \in \{1, 2, \ldots, M-1\}$ is the kmth discrete value of the parameter $\boldsymbol{\Phi}_m$. $\phi_{kM}(SS_n)$ is the kMth discrete value of β_{44} predicted by the GPR model for the sea state SS_n, $\boldsymbol{\Phi}_M = \beta_{44}(SS_n)$.
3. With the pre-established RAO database and the received vessel motion measurements for all the J quantities for the sea state SS_n, the weight matrices can be calculated for each sensor measurement based on the previously described tuning procedure in Section 2.
4. Then the joint probability mass function of vessel parameters can be updated based on Eq. (6), as the posterior of the vessel parameters for the wave information SS_n.
5. The posterior mean $\mu_{\beta_{44}(SS_n)}$ and standard deviation $\sigma_{\beta_{44}(SS_n)}$ can be calculated by

$$PMF^{(pos)}_{SS_n}(\phi_{kM}) = \sum_{k1=1}^{K1} \cdots \sum_{k(M-1)=1}^{K(M-1)} PMF^{(pos)}_{SS_n}(\phi_{k1}, \ldots, \phi_{kM}) \tag{19a}$$

$$\mu^{(pos)}_{\beta_{44}(SS_n)} = \sum_{kM=1}^{KM} \phi_{kM} PMF^{(pos)}_{SS_n}(\phi_{kM}) \tag{19b}$$

$$\sigma^{(pos)}_{\beta_{44}(SS_n)} = \sqrt{\sum_{kM=1}^{KM} (\phi_{kM} - \mu^{(pos)}_{\beta_{44}(SS_n)})^2 PMF(\phi_{kM})} \tag{19c}$$

and the posterior of the other parameters can be calculated for each combination by

$$PMF^{(pos)}_{SS_n}(\phi_{k1}, \ldots, \phi_{k(M-1)}) = \sum_{kM=1}^{KM} PMF^{(pos)}_{SS_n}(\phi_{k1}, \ldots, \phi_{kM}) \tag{20}$$

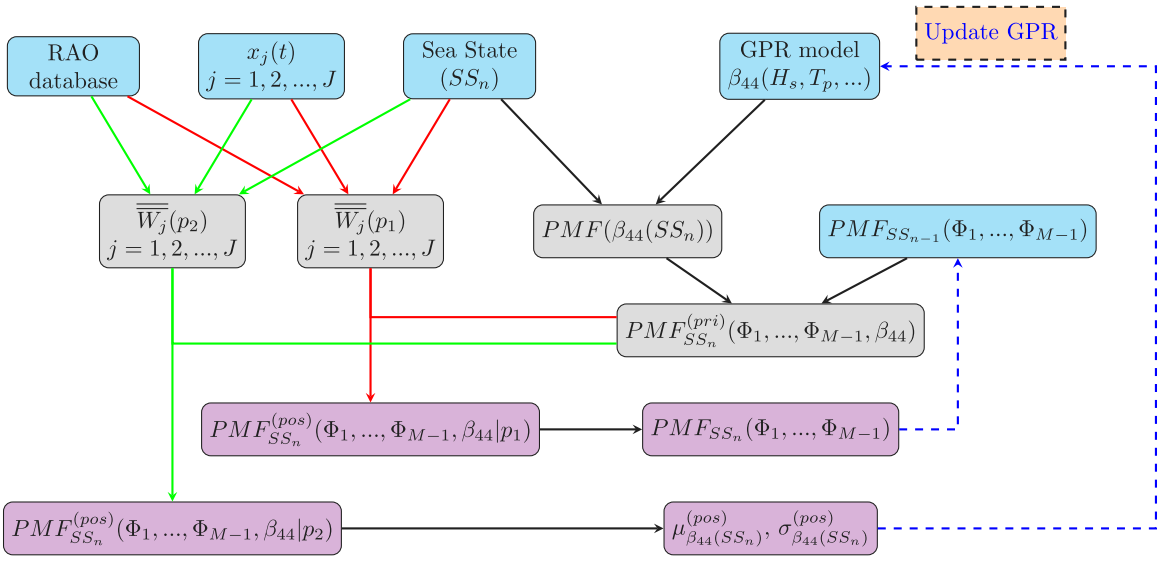

Fig. 4. Process of the 2-step tuning of vessel parameters including sea state dependent β_{44} and updating the β_{44} GPR model, assuming $\Phi_M = \beta_{44}$. Normally $p_1 < p_2$.

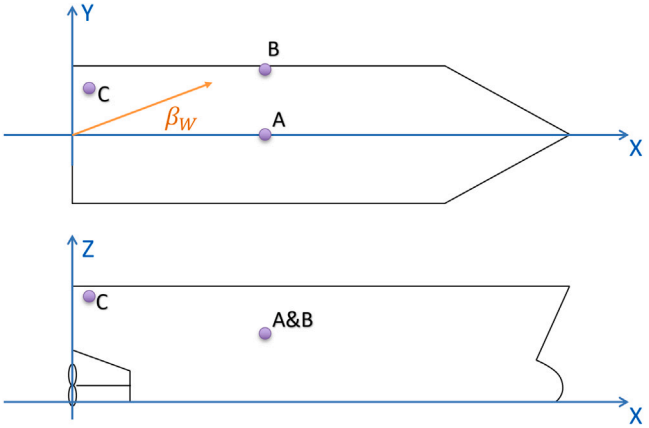

Fig. 5. The reference coordinate system and the locations of the sensors measuring vessel motions such as displacements, velocities, and accelerations.

The GPR model of β_{44} can be updated with the new available information $\mu_{\beta_{44}(SS_n)}^{(pos)}$ and $\sigma_{\beta_{44}(SS_n)}^{(pos)}$.

6. Then for the next sea state, the joint $PMF_{SS_n}^{(pos)}(\Phi_1, \ldots, \Phi_{M-1})$ will become the prior information.

4.2. Two-step tuning procedure

For tuning of sea state dependent parameters, a larger power parameter p is usually desired, due to the very limited number of available measurements for that particular sea state. However, tuning of other parameters may not require (and may not benefit from) application of such a large p value. The larger the p value is, the faster the variance of the parameters can be reduced, potentially leading to an overconfidence issue. The tuning results could be biased (Han et al., 2021a). Once the variance becomes relatively small, the expected value of the tuned parameter becomes very difficult to change.

Considering that all the vessel parameters must be tuned simultaneously, the one-step tuning procedure could be modified by splitting the Bayesian updating into two steps, as illustrated in Fig. 4. The basic idea is to apply two different power parameters, p_1 and p_2 where $p_1 < p_2$, to calculate the $PMF_{SS_n}^{(pos)}(\Phi_1, \ldots, \Phi_{M-1})$ and $PMF_{SS_n}^{(pos)}(\beta_{44})$ separately.

5. Case study basis

Case studies were performed in order to investigate the proposed algorithm in detail. For illustrative purpose, tuning of only 2 vessel parameters simultaneously was considered. The roll damping was assumed to be a function of only three independent wave-related parameters (i.e., H_s, T_p, and β_W), and can be written as a function of two input characteristics (i.e., $H_s \sin\beta_W$ and T_p).

5.1. Vessel information and RAO database

All case studies were based on numerical models for an offshore supply vessel (OSV) close to its ballast condition. Zero forward speed has been considered. The reference coordinate system for the seakeeping analysis is illustrated in Fig. 5. The X–Z plane is at the vessel longitudinal symmetry plane, and the origin is at the stern of the keel elevation. The positive X-axis points towards the bow, the positive Y-axis points towards the port, and the positive Z-axis points vertically upwards. The wave heading β_W, as illustrated in Fig. 5, follows the same coordinate system, in a positive going-to convention.

As described in Section 2, the RAO database should be established to represent the RAOs for all the considered motions, sensor locations, and covering the whole uncertainty ranges for the considered uncertain vessel parameters. The measurements of vessel heave displacements, velocities, and accelerations at three locations (see Fig. 5) have been considered, as summarized in Table 1, assuming that the measurements are independent. It is also assumed that there is much available supplementary information regarding the vessel design properties (e.g., operation design report and arrangement drawing) and onboard sensors (e.g., ballast monitoring) to approximately identify the vessel condition in real time. Therefore, the online vessel model tuning is focused on reducing the uncertainties of the estimated vessel condition resulting from new information becoming available based on measurements. The considered uncertain vessel parameters were selected based on the previous parametric sensitivity study (Han et al., 2020). Their uncertainty ranges are summarized in Table 2. Each of the considered vessel parameters was discretized within the specified uncertainty range. The number of discrete values is also shown in Table 2. In total, 9 wave headings between 30° and 150° with a 15° interval were considered in the RAO database, for all the 9 sensor measurements described in Table 1. All the RAOs were calculated by means of the DNV GL commercial software Wasim (DNV GL, 2018) which is based on application of the Rankine panel method (Kring, 1994).

Table 1
Description of sensor measurements.

Sensor ID	Location	Coordinate (x,y,z) [m]	Signal/measurements
Disp_A	A	(60.0, 0.0, 10.0)	$\eta_3(t)$ at location A
Disp_B	B	(60.0, 13.0, 10.0)	$\eta_3(t)$ at location B
Disp_C	C	(0.0, 10.0, 14.0)	$\eta_3(t)$ at location C
Vel_A	A	(60.0, 0.0, 10.0)	$\dot{\eta}_3(t)$ at location A
Vel_B	B	(60.0, 13.0, 10.0)	$\dot{\eta}_3(t)$ at location B
Vel_C	C	(0.0, 10.0, 14.0)	$\dot{\eta}_3(t)$ at location C
Acc_A	A	(60.0, 0.0, 10.0)	$\ddot{\eta}_3(t)$ at location A
Acc_B	B	(60.0, 13.0, 10.0)	$\ddot{\eta}_3(t)$ at location B
Acc_C	C	(0.0, 10.0, 14.0)	$\ddot{\eta}_3(t)$ at location C

$\eta_3(t)$: time series of heave displacement;
$\dot{\eta}_3(t)$: time series of heave velocity;
$\ddot{\eta}_3(t)$: time series of heave acceleration.

Table 2
Range of vessel model parameters in the RAO database.

Parameters	Variation range	Number of values
Mass	[−6%, +6%]	7
XCG	[−4 m, +4 m]	5
I_{yy}	[−9%, +9%]	7
GMT[a]	[0, 1 m]	6
β_{44}	[2%, 14%]	7

[a]Here "GMT" represents the free surface correction to the transverse metacentric height. $GMT = 0.5$ m here means that the transverse metacentric height is corrected with −0.5 m due to free surface effects. It is not the value of the transverse metacentric height.

Table 3
Data points for building the linear function of β_{44}.

T_p [s]	ω_p [rad/s]	$H_s \sin\beta_W$ [m]	β_{44} [–]
5	1.2566	0.0	0.04
25	0.2513	0.0	0.03
5	1.2566	1.0	0.05
25	0.2513	1.0	0.03
5	1.2566	2.0	0.065
25	0.2513	2.0	0.03
5	1.2566	4.0	0.08
25	0.2513	4.0	0.03

5.2. Assumed function of additional roll damping

As discussed in Section 1, the linearized roll damping B_{44} can be a function of many parameters, e.g.,

$$B_{44} \sim g(H_s, T_p, \beta_W, COG, mass, u, \phi_A ...) \tag{21}$$

where COG is the vessel centre of gravity, $mass$ is the vessel mass. In real applications, the GPR model of the roll damping B_{44} can be initiated based on the Ikeda's formulas mentioned in Section 1. Then the acquired wave and vessel motion measurements can assist in tuning B_{44} and updating the GPR model according to the proposed procedures in Section 4. For the purpose of demonstration, it was assumed that the roll damping according to the potential theory has been accurately calculated by seakeeping analysis software, and the linearized additional roll damping coefficient β_{44} can be accurately described as:

$$\beta_{44} \sim f(H_s \sin\beta_W, \omega_p) \tag{22a}$$

$$\beta_{44} = \frac{B_{44} - B_W}{B_{44,crit}} \tag{22b}$$

where $f()$ is a linear function, $\omega_p = \frac{2\pi}{T_p}$, $B_{44,crit}$ is the critical roll damping calculated based on vessel hydrodynamic coefficient matrices of added mass, inertia, and stiffness. The true linear function $f()$, illustrated in Fig. 6, was defined by the data points as summarized in Table 3. Linear interpolation between the data points was applied. Extrapolation was not allowed.

Table 4
Prior information and true values of GMT and XCG.

Case ID	Parameter	Mean	σ^2	True value
Case_GMT	GMT [m]	0.5	0.015	0.6
Case_XCG	XCG [m]	59.4	1.21	57.4

The prior knowledge about β_{44} was considered as a constant Gaussian process, with prior mean of 0.07 and variance of 0.02^2 i.e.,

$$\beta_{44,0} \sim \mathcal{N}(0.07, 0.02^2) \tag{23}$$

The prior mean and prior variance of β_{44} is also illustrated in Fig. 6.

5.3. Scope of case studies

Two separate cases were studied in detail. Case_GMT investigated the algorithm performance for tuning of GMT and β_{44} and updating the prediction model for β_{44} simultaneously, whereas, Case_XCG investigated the algorithm performance for tuning of XCG and β_{44} and updating the prediction model for β_{44} simultaneously. The prior and true β_{44} are described in Section 5.2. For demonstration purposes, the assumed true values and prior knowledge about the GMT and XCG in the case studies are defined in Table 4. Demonstration on tuning and prediction of β_{44} is the key objective of the case studies. Therefore, no head seas or following seas have been considered.

It is worth mentioning that the proposed GPR model can also be used for designing experimental test scopes actively, i.e., an adaptive sequential experimental design, e.g., Neumann-Brosig et al. (2020). Based on available experimental data, the GPR model can indicate where the largest uncertainty is to be found. Consequently the next test can be designed at that point to optimize the test scope. However, for the vessel in operations, the occurrence of sea states is decided by nature. Consequently, the sampling scheme cannot be established in the same way as for adaptive sequential experimental design. For the case studies, the sea states were randomly simulated as shown in Table 5. Similar to the case studies demonstrated by Han et al. (2021a,b), H_s, T_p, and β_W were also assumed to be evenly distributed random variables within the specified ranges, only for demonstration purposes. Note that the variables which represent the long-term wave conditions are usually not uniformly distributed in the real world. All the sea states were assumed to be adequately represented by the Pierson–Moskowitz (PM) spectrum. Directional spreading of the sea states was not considered.

Many initial simulations were performed in order to understand how the proposed algorithms will work. The initial findings were:

1. More samples are required in order to train the GPR model for the case of higher dimension. The considered GPR model actually have 3 random input parameters, i.e., ω_p, H_s, and β_W. The random generation of the uniformly and independently distributed H_s and β_W variables actually leads to a non-uniformly distributed $H_s \sin\beta_W$. Consequently, a much smaller likelihood of occurrence should be expected along the edges of the considered surface of the β_{44} GPR model.
2. For the β_{44} GPR model, the prior variance described in Eq. (23) should be applied as the hyperparameter signal variance (σ_f^2).
3. Each of the two input characteristics of the GPR model (i.e., $H_s \sin\beta_W$ and ω_p) requires an independent length-scale l. For an uncomplicated and smooth true surface such as a polynomial function, it seems reasonable to set l to be 10%–20% of the total range of each axis parameter.
4. For sea state SS_n, the variance of $\beta_{44}(SS_n)$ after tuning represents the uncertainty of that data point. Therefore, $\sigma_y(SS_n) = \sigma^{(pos)}_{\beta_{44}(SS_n)}$.
5. Tuning of the sea state dependent β_{44} requires a relatively large power parameter p.

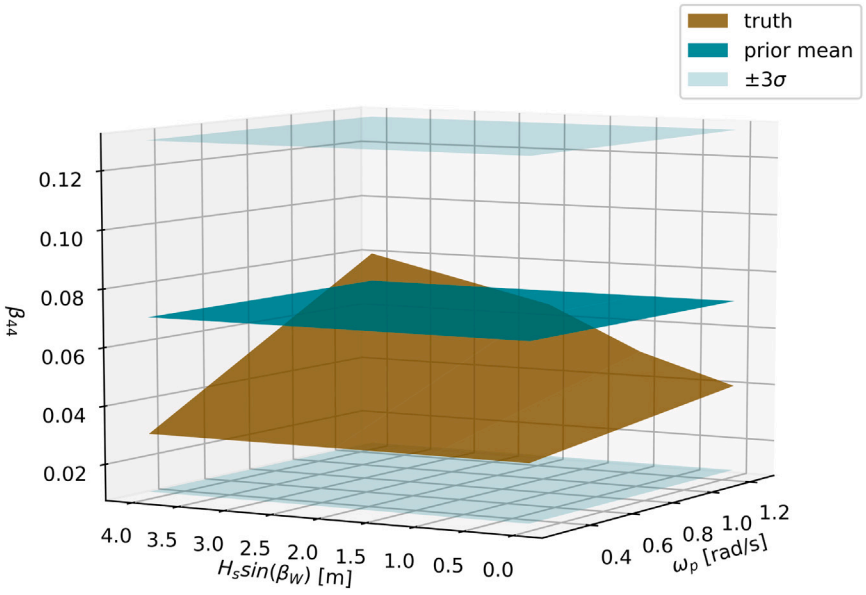

Fig. 6. The true function surface of $\beta_{44}(H_s \sin\beta_W, \omega_p)$ and the associated prior knowledge.

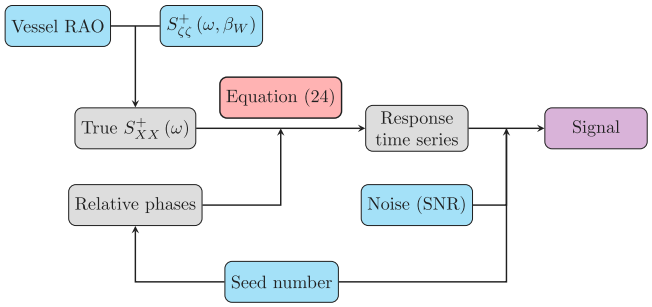

Fig. 7. Flow chart for the purpose of simulating noisy vessel response measurements.

The vessel motion signals were numerically simulated. Noise was also added to the signals. The considered input parameters for noisy signal simulation and case studies are summarized in Table 5. The vessel motion measurements for each sea state were simulated for 1 h. Each case study included 72 sea states. The procedure of simulating the noisy vessel motion measurements is illustrated in Fig. 7. The true response spectrum for response X, i.e., $S^+_{XX}(\omega)$ can be calculated based on the wave spectrum of the randomly simulated sea state and the corresponding vessel response RAO. A realization of that response can be generated by:

$$x(t) = \sum_{n=1}^{N_\omega} C_n(\omega_n) \cos(\omega_n t + \varphi_n) \tag{24a}$$

$$C_n(\omega_n) = \sqrt{2 S^+_{XX}(\omega_n) \cdot \Delta\omega} \tag{24b}$$

where $\varphi_n \in [0, 2\pi)$ is a random phase angle which is continuous and uniformly distributed, $\Delta\omega$ is the interval of the discrete radial frequencies ω_n, and N_ω is the total number of discrete frequencies for the response spectrum. Then the signal noise can be added to each time step of the time series, assuming that (1) the signal noise is white noise, i.e., $WN \sim \mathcal{N}(0, \sigma_N^2)$; (2) and the variance of noise σ_N^2 is proportional to the true signal variance σ_X^2, defined as SNR (signal-to-noise ratio).

$$SNR = \frac{\sigma_X^2}{\sigma_N^2} \tag{25}$$

Table 5
Applied parameters related to the signal simulation, model tuning, and GPR model fitting.

Parameter	Value
H_s	Uniformly distributed in [1.0, 4.0] m
T_p	Uniformly distributed in [5.0, 25.0] s
β_W	Randomly selected among 9 discrete directions within [30°, 150°]
Seeds	Randomly generated within [1, 300]
Duration	3600 s
SNR	30
α	0.05
f_{lp}	0.2 Hz
p	0.6*
$l(H_s \sin\beta_W)$	0.7 m
$l(\omega_p)$	0.2 rad/s
σ_f^2	0.02^2

*$p = 0.6$ was applied to the case studies for the 1-step tuning procedure. $p_1 = 0.3$ and $p_2 = 0.7$ were applied to the case studies for the 2-step tuning procedure.

6. Results

6.1. One-step tuning

A number of cases have been analysed, also including stochastic variability obtained by means of seed variation. A summary of the aggregated results are reported for the purpose of demonstration and documentation of the algorithm performance.

6.1.1. Case_GMT

Representative results corresponding to two different realizations are included, with initial seed number 128 (denoted as "Seed128") and seed number 45 (denoted as "Seed45"). Note that different initial seed number will determine different sea states with respect to different H_s, T_p, β_W, and seeds for generating virtual noisy signals. Figs. 8 and 9 illustrate the updated GPR model for β_{44} after tuning the vessel parameters for 72 sea states. Information on the randomly generated sea states and the intermediate results with respect to tuning of β_{44} are summarized in Tables A.6 and A.7 in Appendix for Seed128 and Seed45 respectively. The expected values of the tuned β_{44} for those 72 sea states are also illustrated as samples in Figs. 8 and 9. Figs. 10 and 11 illustrate the tuned results of GMT throughout the 72 sea states for Seed128 and Seed45, respectively. As expected, both β_{44} GPR models

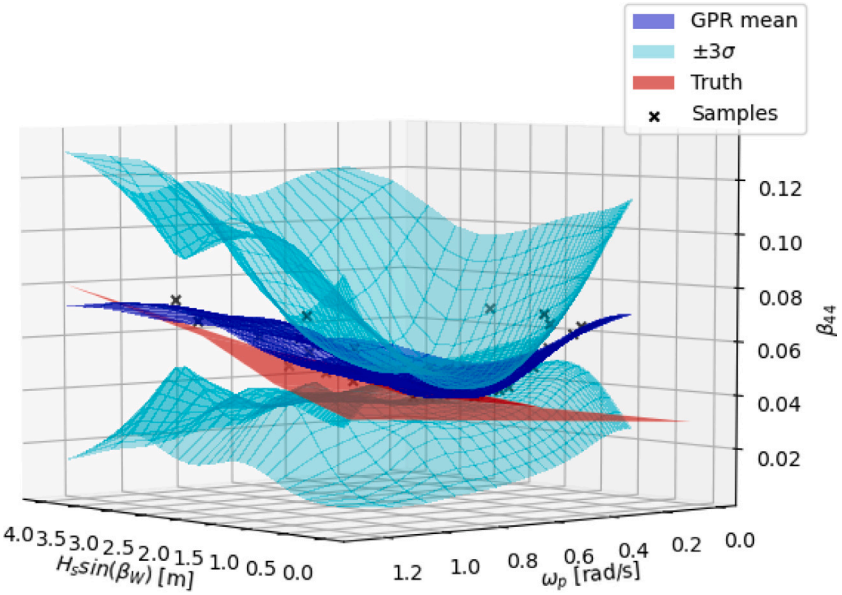

Fig. 8. The updated β_{44} GPR model after tuning of β_{44} and GMT for 72 sea states, for Seed128.

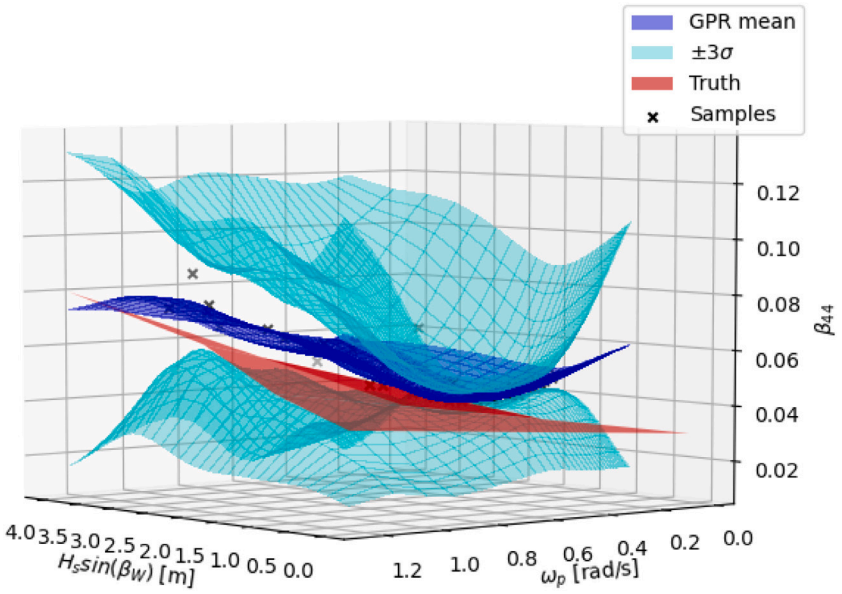

Fig. 9. The updated β_{44} GPR model after tuning of β_{44} and GMT for 72 sea states, for Seed45.

are found to converge towards the presumably true function. The posterior knowledge on β_{44}, in terms of the mean and variance, improves significantly based on the simulated vessel motion measurements for 3 days. However, the results of the tuned GMT become very different for the two presented cases. For Seed128 case (Fig. 10), the GMT mean fluctuates around the true value. When the tuning algorithm finds that the previously tuned GMT deviates significantly from the current observation, the variance dramatically increases, reflecting the confusion of the system. The increasing variance helps the system to adjust the tuning direction. Note that more simulations with different initial seeds were performed. For most simulated cases, the tuned GMT fluctuates about 0.5 m and 0.6 m throughout the 72 sea states, similarly to the behaviour illustrated in Fig. 10. On the contrary, Fig. 11 shows that the tuned GMT for case Seed45 significantly deviates from the true value. The variance was reduced significantly, while the mean value of the GMT was quickly tuned to a wrong value. This leads to an over-confident situation, where the tuning system was not able to bounce back to the true value. As shown in Fig. 11, the variance increased significantly between sea state number 45 and 50, and sea state number 66 and 68. The system tried very hard to bounce back towards the true value. However, it did not manage to change the tuned mean value of the GMT significantly.

This type of over-confidence is dangerous. Hence, a too rapid decrease of the variance for parameters that are not sea state dependent should be avoided. The bias associated with the tuned value of the GMT also indicates that the GMT may not be very sensitive to vessel motions for most wave conditions.

It is worth mentioning that the sequence of the occurring sea states and the corresponding measurements can influence the tuning of the sea state independent parameters (i.e., GMT in this case) as well as the updated GPR model for the sea state dependent β_{44}. However, such influence is usually very limited for convergent tuning results with sufficient amount of data and carefully selected power parameter

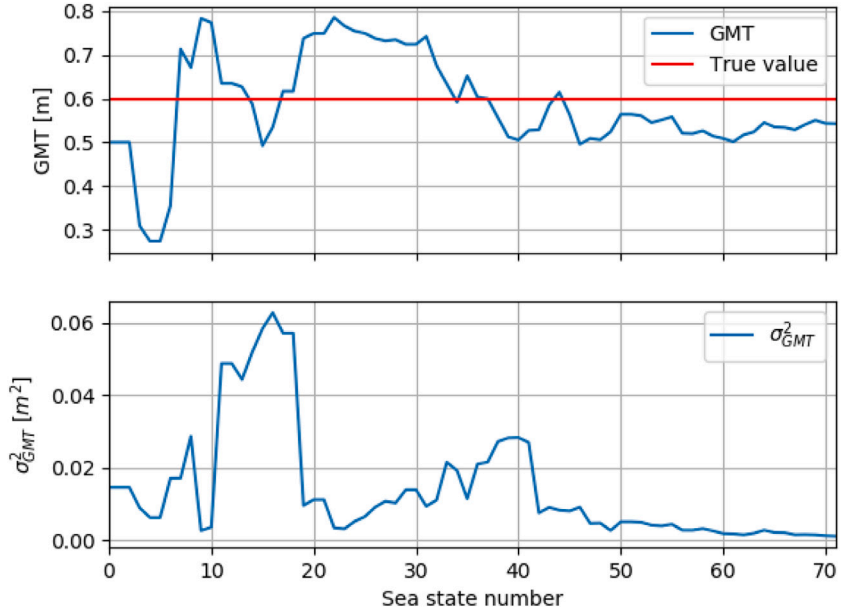

Fig. 10. The mean and the variance of the tuned GMT through the simulated 72 sea states, for Seed128.

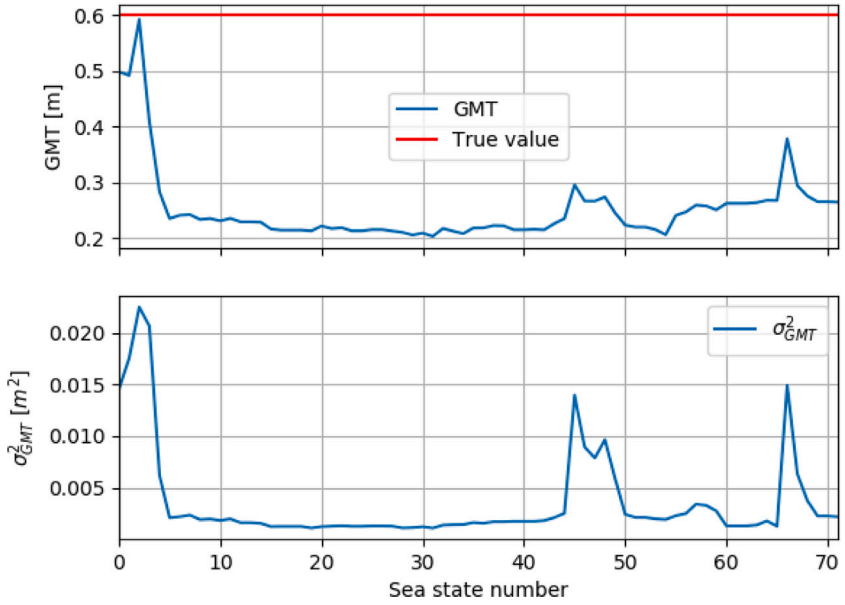

Fig. 11. The mean and the variance of the tuned GMT through the simulated 72 sea states, for Seed45.

p so that over-confident tuning can be avoided. Divergent tuning results, however, can be more influenced by the order of the sea state occurrence. In reality, the tuning is carried out in the sequence of occurrence by nature, which means that changing the tuning sequence is not relevant in practice.

6.1.2. Case_XCG

Based on earlier studies (Han et al., 2020, 2021a,c), the value of XCG is found to have a stronger influence on the vessel motions than the value of GMT. Therefore, as expected, tuning of XCG was much more stable than tuning of GMT. Fig. 12 shows the significantly improved GPR model of β_{44}, compared with the prior knowledge (Fig. 6). The intermediate tuning results of β_{44} are summarized in Table A.8 in Appendix. Fig. 13 shows that the tuned XCG gradually approaches the true value.

6.2. Two-step tuning

Based on the findings in Section 6.1.1, the over-confidence (low variance) implies that the 1-step parameter tuning procedure has difficulties in counteracting the convergence to the wrong value. Therefore, it is of great interest to apply the proposed 2-step tuning procedure, as described in Section 4.2, so that the sea state independent vessel parameters can be tuned relatively slowly.

Compared with results based on the 1-step tuning procedure, the trained GPR models of β_{44} approach the true surface in a better way, due to the applied higher power parameter for tuning of β_{44}. Tables A.9 and A.10 in Appendix summarize the intermediate tuning results of β_{44} for Case_GMT (Seed45) and Case_XCG (Seed128), respectively, based on 2-step tuning procedure.

With respect to tuning of GMT, as shown in Fig. 14, the 2-step tuning algorithm by application of a smaller power parameter leads

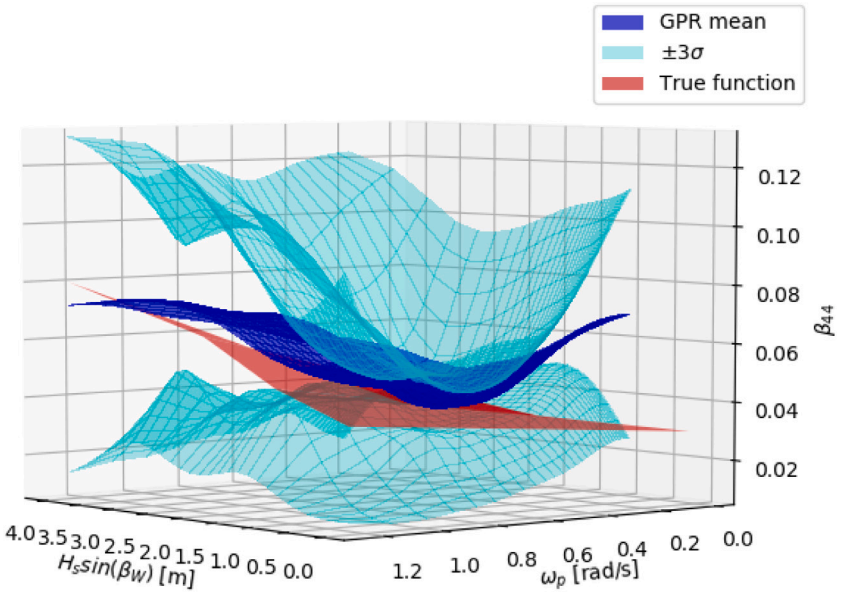

Fig. 12. The updated β_{44} GPR model after tuning of β_{44} and XCG for 72 sea states, for Seed128.

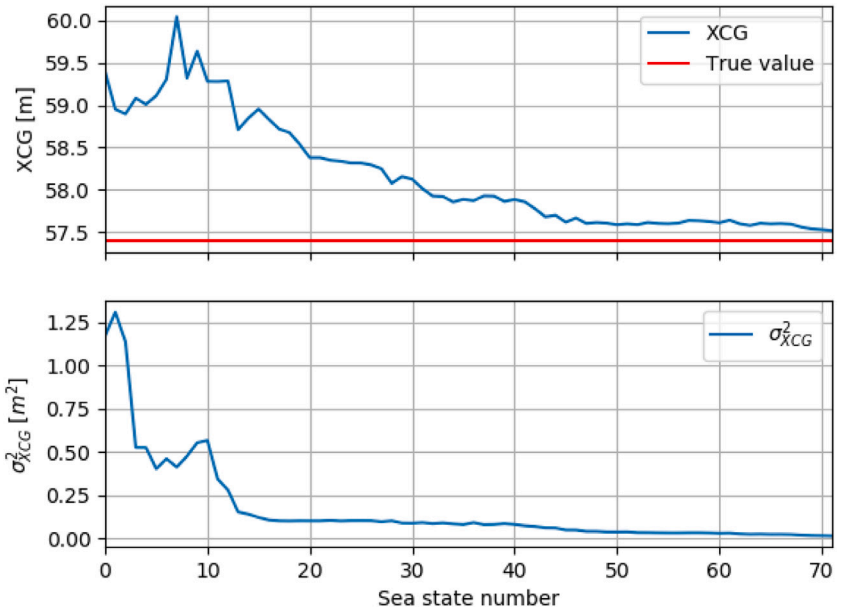

Fig. 13. The mean and the variance of the tuned XCG through the simulated 72 sea states, for Seed128.

to smaller fluctuations of the tuned mean values based on the measurements from different sea states. The over-confidence issue with respect to the GMT variance could therefore mainly be avoided. A large variance is preferred instead of a biased estimate resulting from over-confidence due to a fictitiously small variance.

As shown in Fig. 15, with a smaller power parameter p, tuning of the XCG was even accelerated towards the true value approximately between sea state number 15 and 40. The variance decreased more slowly, but the expected value converged faster towards the true value.

7. Conclusions and future work

The paper has proposed an algorithm for tuning and prediction of sea state dependent roll damping by an iterative closed loop between the tuning procedure and the GPR based prediction model. The tuned β_{44} for the current sea state updates the GPR model which in return improves the β_{44} prediction for future sea states. A simple and representative roll damping function was presumed for the numerical studies for demonstration purposes. The numerical case studies have shown that the tuning procedure succeeds to improve the roll damping coefficient estimation. The true variation of β_{44} is expected to be identified based on the real on-site vessel motion measurements and the environment, although subjected to some uncertainties.

With the 1-step tuning algorithm, the sea state independent parameters such as GMT and XCG may suffer from the over-confidence issue due to the applied large power parameter. Therefore, a 2-step tuning algorithm was proposed by applying two sets of different likelihood functions to update the prior knowledge, in order to tune roll damping and other parameters with different confidence level. Case studies showed that the 2-step tuning algorithm may even accelerate the tuning towards the true value. In addition, for the biased tuning (e.g., tuning of GMT for initial seed number of 45) the 2-step tuning can at least slow down the divergence.

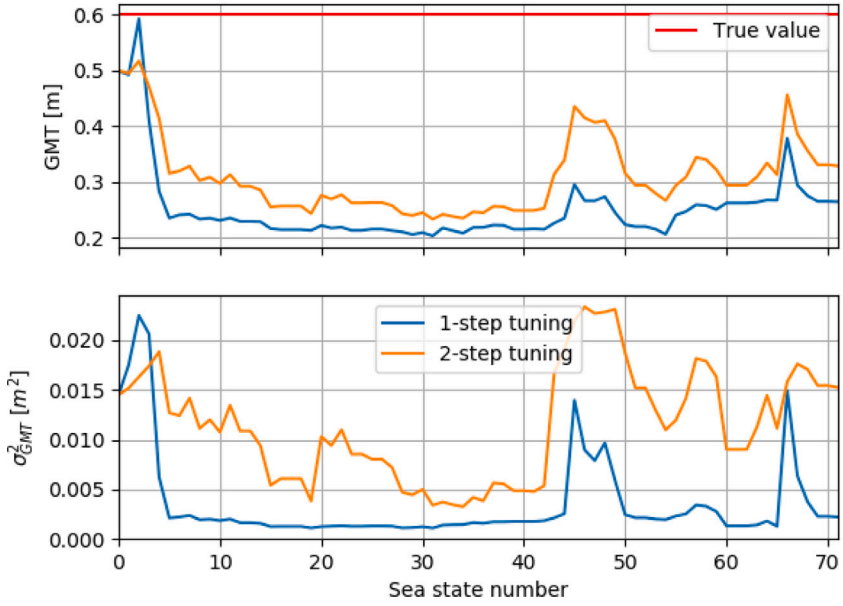

Fig. 14. Comparison of the mean and the variance of the tuned GMT through the simulated 72 sea states obtained respectively by application of the 1-step and the 2-step tuning procedures, for Seed45.

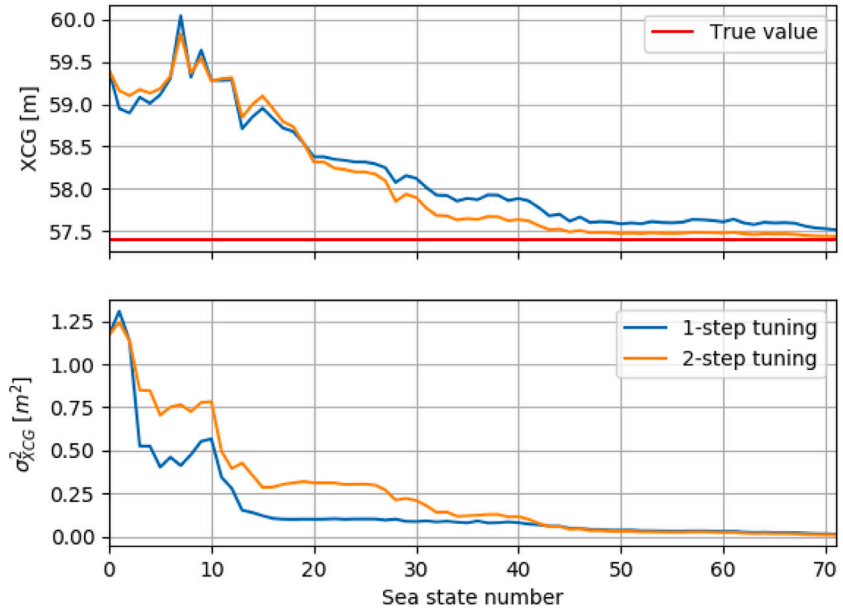

Fig. 15. Comparison of the mean and the variance of the tuned XCG through the simulated 72 sea states obtained respectively by application of the 1-step and the 2-step tuning procedures, for Seed128.

Even though the proposed tuning framework is expected to improve the estimation of sea state dependent vessel parameters, several important limitations should be emphasized for real applications:

1. The amount of on-site measurements can be limited especially for operations with frequently changing vessel conditions. There might be only a few available sea states for a certain vessel condition with respect to inertia distribution and vessel speed. Therefore, it might be reasonable to apply larger length-scale l in the RBF kernel of the GPR model in order to make the available updates influence the GPR model as much as possible. However, "under-fitting" may occur, as illustrated in Fig. 2.
2. The proposed algorithm for online tuning of sea state and vessel condition dependent roll damping based on on-site measurements cannot fully substitute lab experiments. The vessels are designed to survive at extreme and accidental scenarios, which probably do not happen on-site for a considerably long period. Therefore, tuning based on on-site measurements is probably insufficient to find a complete and sufficiently accurate function for representation of roll damping, covering the most extreme weather conditions and accidental scenarios. Lab tests can be designed and optimized, but not for on-site conditions. Using on-site measurements to improve the knowledge of roll damping for moderate seas is reasonable. However, predicting the extremes should still rely on model tests and CFD analysis.

3. The on-site sea states usually vary slowly, meaning that the sea state occurring afterwards is normally close to the current sea state. This slowly-varying characteristics negatively influence the global performance of the GPR model updating. However, this could also be an advantage in terms of better accuracy in relation to the local input domain of highest interest. More useful data can be available in a concentrated sub-space of the input parameters (e.g. H_s and T_p), and the environmental condition for the operation in the near future is probably located close to or within this concentrated input space. Consequently, more confidence could be obtained within such input space of great interest for the near future operation.

In addition, future work is essentially required before real applications on board can be achieved:

1. As stated in Items 2 and 3 of the algorithm limitations, the probability of occurrence for wave conditions is not uniformly distributed in the real world. Hence, insufficient observations with respect to GPR modelling are expected at those wave conditions with low probability of occurrence. The RBF kernel may be modified so that the length-scale l can be location dependent in the input space of the GPR model. A larger value of l may be applied for the input sub-space with low probability of occurrence so that those less frequently observed samples can have increased influence on a wider range of the input domain.
2. The proposed tuning framework as described in Section 4 introduces a GPR model which relies on the selection of the kernel and its hyperparameters. The hyperparameters of the GPR model can be optimized as described in Section 3. However, it was found that the optimal solution depends on the initial searching values, bounds, the amount of training data, and the applied algorithm (Erickson et al., 2018). Therefore, future research should investigate the effects of applying other kernels (e.g., Matérn kernel, Rational quadratic kernel, and Dot-Product kernel) and the effects of applying the automatic tuning of the kernel's hyperparameters on the results of tuning and predicting vessel parameters.
3. The GPR prediction model must be continuously quality checked. Usually a stopping criterion should be introduced in the future to avoid analysis divergence. For the β_{44} GPR model, the stopping criterion could be related to the prediction error. For example, if the tuned roll damping based on the new measurements is outside of the 99-percentile interval of the available GPR model at that sea state, then it might indicate that (1) the GPR model is over-confident; (2) the tuned results are biased; or (3) the vessel condition is changed, etc.
4. Roll damping depends not only on the sea states, but also on the vessel conditions such as vessel forward speed and loading conditions. Future research should demonstrate the tuning algorithm with a more complete roll damping GPR model which is sea state and vessel condition dependent. The proposed procedure could be modified by just including parameters with respect to vessel conditions as input parameters to the GPR model.
5. In reality, the acquired wave information e.g., on H_s and T_p, is always subject to uncertainties, which was not considered in the present paper. It is important as part of future work to systematically consider the effects of the weather uncertainties on the model tuning algorithm and the roll damping GPR model.
6. In the tuning procedure, the values of the power parameter p and the SSR criterion parameter α_0 can significantly influence the tuning results, and the selection of both values is at the moment based on trial and error. How to determine their values based on available quantitative information about system dimension, measurement uncertainty, etc., can be important to investigate as part of future work.

Nomenclature

Abbreviations

CFD	Computational Fluid Dynamics
COG	Centre of gravity
GMT	Correction to the transverse metacentric height due to free surface effects
GPR	Gaussian process regression
ITTC	International Towing Tank Conference
OSV	Offshore supply vessel
PDF	Probability density function
PM	Pierson–Moskowitz spectrum
PMF	Probability mass function
RAO	Response amplitude operator
RBF	Radial-basis function
SNR	Signal-to-noise ratio
SSR	Sensor screening ratio
WN	White noise
XCG	Longitudinal coordinate of vessel centre of gravity

Vectors and matrices

$\bar{\boldsymbol{\mu}}_*$	The conditional mean for the prediction space with the given observations
$\bar{\boldsymbol{K}}_{**}$	The updated kernel for the prediction space with the given observations
$\boldsymbol{\epsilon}$	The noise of the observations $\tilde{\boldsymbol{Y}}$
$\boldsymbol{\mu}_*$	The prior mean for the prediction space
$\boldsymbol{\mu}_Y$	The prior mean for the input space
$\boldsymbol{K}_{**}$	The prior covariance for the prediction space
$\boldsymbol{K}_{\tilde{Y}}$	The kernel for the input space with noise
$\boldsymbol{K}_{Y*}$	The kernel between input and prediction spaces
$\boldsymbol{K}_Y$	The kernel for the input space
$\underline{\boldsymbol{y}_*}$	The prediction space for the function $y = f(x)$ at $\boldsymbol{x} = \boldsymbol{x}_*$
$\overline{\overline{W}_j}$	The weight matrix (likelihood function) based on the received measurements $x_j(t)$
$\tilde{\boldsymbol{Y}}$	The observations related to the input space $\boldsymbol{Y}$

Other Symbols

α_j	Sensor screening ratio (SSR) for the measured quantity j
β_{44}	Ratio between the additional roll damping and the critical roll damping
β_W	Wave direction w.r.t. vessel coordinate system
$\eta_3, \dot{\eta}_3, \ddot{\eta}_3$	Heave displacement, velocity, acceleration
ω	Wave frequency
ω_p	Wave spectral peak frequency
ϕ_A	Roll amplitude
$\boldsymbol{\Phi}_m$	The uncertain vessel parameter to be tuned, $m \in \{1, 2, ..., M\}$
ϕ_{im}	The imth discrete value of the vessel parameter $\boldsymbol{\Phi}_m$ in the RAO database
ϕ_{km}	The kmth discrete value of the vessel parameter $\boldsymbol{\Phi}_m$ in the discrete joint probability distribution
$\sigma^2_{y_i}$	The variance of the observation y_i
σ^2_N	Variance of noise
σ^2_X	Variance of response
σ^2_f	Signal variance
$\sigma_{\sigma_{r,j}}$	The standard deviation of $\sigma_{r,j}$ over $r \in \{1, 2, ldots, R\}$
$\sigma_{r,j}$	The predicted standard deviation by using $RAO_{r,j}$
$\hat{\sigma}_j$	The standard deviation of the filtered signal $\hat{x}_j(t)$
B_{44}	Roll damping
B_{BK}	The damping component of B_{44} due to bilge keels
B_E	The damping component of B_{44} due to eddy making
B_F	Friction damping component of B_{44}
B_L	Linear lift damping component of B_{44}
B_W	Wave damping component of B_{44}
f_{lp}	lowpass filter cutoff frequency [Hz]

$H_{r,j}(\omega,\beta_W)$	Linear transfer function between wave and vessel (heave) response for the measured quantity j based on the combination r for the uncertain vessel parameters, i.e. $RAO_{r,j}$
H_s	Significant wave height
Im	The number of discrete values used for RAO database for the vessel parameter Φ_m
im	The imth value of the variable Φ_m in the RAO database
J	The total number of the measured quantities
j	The index of the measured quantities, representing different motions and their derivatives (i.e., displacement, velocity, acceleration) at various locations
Km	The number of discrete values used for the probability distribution model for the vessel parameter Φ_m
km	The kmth value of the discretized variable Φ_m in the probability distribution model
l	Length-scale
M	The number of considered variables for tuning
N_ω	The number of discretized frequencies
N_t	The number of discretized time steps
N_{Prob}	The total number of the discrete points for the joint probability distribution, $N_{Prob}=\prod_{m=1}^{M}(Km)$
p	Power parameter
R	The total number of possible vessel parameter combinations to build the RAO database, $R=\prod_{m=1}^{M}(Im)$
$RAO_{r,j}$	The RAO based on the variable combination r, for the measured quantity j, i.e., $H_{r,j}(\omega,\beta_W)$
$S^{+}_{\zeta\zeta}(\omega,\beta_W)$	Single-sided power spectral density of long-crested waves
$S^{+}_{XX}(\omega)$	Single-sided power spectral density of vessel response X
SS_n	The index of the occurring sea state, i.e., the sea state number
T_p	Spectral peak period
u	Vessel forward speed
$w_{r,j}$	Weight factor for the rth variable combination based on measurement of quantity j
$x_j(t)$	The original signal for the measured quantity j at time step t
$\bar{x}_j$	The mean of the filtered time series $\hat{x}_j(t)$
$\hat{x}_j(t)$	The filtered time series of $x_j(t)$

CRediT authorship contribution statement

Xu Han: Conceptualization, Methodology, Software, Formal analysis, Data curation, Writing - original draft, Writing - review & editing. **Svein Sævik:** Writing - review & editing, Supervision, Project administration. **Bernt Johan Leira:** Writing - review & editing, Supervision, Project administration, Funding acquisition.

Declaration of competing interest

The authors declare that they have no known competing financial interests or personal relationships that could have appeared to influence the work reported in this paper.

Acknowledgements

This work was made possible through the Centre for Research based Innovation MOVE, financially supported by the Research Council of Norway, NFR project no. 237929 and the consortium partners, http://www.ntnu.edu/move. Special thanks are given to Section of Hydrodynamics & Stability in DNV for providing the numerical seakeeping models.

Appendix. The simulated sea states and tuning of β_{44}

The parameters summarized in the tables are described as follows:

- SS_n: sea state number (index)
- H_s [m]: significant wave height
- β_W [°]: wave direction
- T_p [s]: wave spectral peak period
- β^*_{44}: the true value of β_{44} according to Table 3
- $\bar{\beta}_{44}$: the GPR model predicted β_{44} before tuning for sea state SS_n
- $\bar{\sigma}^2_{\beta_{44}}$: the GPR model predicted variance of β_{44} before tuning for sea state SS_n
- $\hat{\beta}_{44}$: the tuned β_{44} for sea state SS_n
- $\hat{\sigma}^2_{\beta_{44}}$: the variance of β_{44} after tuning for sea state SS_n

Table A.6
The simulated sea states and the tuning inputs and outputs of β_{44} — Case_GMT for Seed128 with 1-step tuning.

SS_n	H_s	β_W	T_p	β^*_{44}	$\bar{\beta}_{44}$	$\bar{\sigma}^2_{\beta_{44}}$	$\hat{\beta}_{44}$	$\hat{\sigma}^2_{\beta_{44}}$
1	3.60	150	22.59	0.0366	0.0700	4.0E−04	0.0700	3.9E−04
2	1.79	30	19.40	0.0346	0.0700	4.0E−04	0.0700	3.9E−04
3	1.39	45	22.73	0.0341	0.0700	4.0E−04	0.0658	3.9E−04
4	1.12	75	15.63	0.0365	0.0690	1.9E−04	0.0428	2.0E−05
5	1.72	90	20.17	0.0372	0.0597	1.5E−04	0.0442	3.9E−05
6	2.94	150	20.40	0.0362	0.0467	3.6E−05	0.0467	3.5E−05
7	3.37	90	15.17	0.0443	0.0694	4.0E−04	0.0435	4.4E−05
8	2.80	90	15.59	0.0426	0.0494	1.9E−04	0.0411	1.5E−05
9	2.00	45	17.27	0.0372	0.0430	2.1E−05	0.0424	1.7E−05
10	1.36	105	11.12	0.0408	0.0462	1.9E−04	0.0412	1.7E−05
11	1.93	135	16.25	0.0375	0.0411	1.0E−05	0.0410	8.5E−06
12	1.33	120	15.00	0.0371	0.0420	9.8E−06	0.0416	7.7E−06
13	2.81	150	18.00	0.0369	0.0437	5.1E−06	0.0437	4.9E−06
14	1.75	75	6.48	0.0533	0.0685	3.9E−04	0.0713	2.3E−04
15	1.90	120	7.72	0.0490	0.0641	1.9E−04	0.0585	1.3E−04
16	2.55	120	8.27	0.0518	0.0605	2.4E−04	0.0587	1.1E−04
17	3.15	60	8.94	0.0523	0.0579	2.0E−04	0.0540	8.9E−05
18	3.79	60	13.38	0.0461	0.0442	5.2E−05	0.0451	3.5E−05
19	1.31	30	24.86	0.0331	0.0654	1.6E−04	0.0654	1.5E−04
20	3.12	60	11.44	0.0471	0.0450	7.6E−05	0.0420	2.0E−05
21	3.96	60	8.82	0.0555	0.0599	2.2E−04	0.0584	5.5E−05
22	2.68	150	22.73	0.0351	0.0518	2.4E−05	0.0518	2.3E−05
23	2.78	135	14.87	0.0411	0.0399	6.5E−05	0.0409	2.9E−05
24	3.23	90	22.04	0.0393	0.0499	1.1E−04	0.0420	2.2E−05
25	3.46	90	24.63	0.0386	0.0464	5.2E−05	0.0432	2.6E−05
26	1.38	105	22.24	0.0352	0.0511	9.5E−06	0.0504	9.0E−06
27	3.72	135	22.40	0.0382	0.0472	6.8E−05	0.0457	5.4E−05
28	2.72	30	17.03	0.0371	0.0423	2.0E−06	0.0423	2.0E−06
29	3.19	45	10.69	0.0469	0.0447	4.8E−05	0.0441	3.2E−05
30	1.90	135	20.10	0.0359	0.0475	2.1E−06	0.0474	2.1E−06
31	1.20	30	21.08	0.0335	0.0630	7.1E−05	0.0630	6.8E−05
32	1.49	30	9.75	0.0388	0.0547	1.8E−04	0.0440	5.3E−05
33	1.40	60	8.80	0.0430	0.0502	6.2E−05	0.0431	1.9E−05
34	2.97	105	24.73	0.0377	0.0454	3.1E−05	0.0437	2.2E−05
35	2.27	135	12.44	0.0413	0.0391	1.6E−05	0.0395	1.0E−05
36	3.95	90	13.38	0.0479	0.0568	1.7E−04	0.0444	4.1E−05
37	2.21	105	23.40	0.0371	0.0496	4.3E−05	0.0458	2.8E−05
38	1.76	45	21.29	0.0352	0.0504	2.8E−06	0.0503	2.7E−06
39	1.65	105	21.79	0.0362	0.0477	5.8E−06	0.0471	5.4E−06
40	3.53	120	5.73	0.0673	0.0706	3.8E−04	0.0751	1.1E−04
41	3.07	45	23.35	0.0372	0.0469	1.5E−05	0.0465	1.4E−05
42	1.61	120	6.32	0.0504	0.0667	1.6E−04	0.0615	6.1E−05
43	3.12	75	17.62	0.0415	0.0416	9.6E−06	0.0408	4.8E−06
44	3.52	30	12.51	0.0422	0.0401	8.5E−06	0.0401	6.1E−06
45	3.24	90	12.25	0.0475	0.0452	2.1E−05	0.0437	1.4E−05
46	3.25	60	5.83	0.0651	0.0744	1.1E−04	0.0675	7.6E−05
47	1.67	75	17.27	0.0380	0.0416	2.8E−06	0.0412	2.2E−06
48	1.72	60	11.88	0.0412	0.0395	4.8E−06	0.0398	3.0E−06
49	3.63	60	24.95	0.0380	0.0434	1.1E−05	0.0430	9.4E−06
50	3.61	105	17.85	0.0423	0.0421	1.6E−05	0.0411	7.7E−06
51	2.83	75	13.71	0.0443	0.0409	8.8E−06	0.0407	5.2E−06
52	1.62	150	16.24	0.0353	0.0508	1.9E−05	0.0508	1.8E−05
53	1.62	30	10.67	0.0383	0.0434	3.0E−05	0.0422	1.9E−05
54	2.31	60	18.50	0.0389	0.0426	5.6E−06	0.0421	4.7E−06
55	2.70	135	21.01	0.0375	0.0450	2.7E−06	0.0449	2.5E−06

(*continued on next page*)

Table A.6 (*continued*).

SS_n	H_s	β_W	T_p	β^*_{44}	$\bar{\beta}_{44}$	$\bar{\sigma}^2_{\beta_{44}}$	$\hat{\beta}_{44}$	$\hat{\sigma}^2_{\beta_{44}}$
56	3.27	60	22.06	0.0387	0.0431	5.4E−06	0.0427	4.9E−06
57	2.55	75	24.19	0.0373	0.0458	6.7E−06	0.0447	6.0E−06
58	3.06	45	20.93	0.0381	0.0441	2.0E−06	0.0440	2.0E−06
59	1.77	120	8.54	0.0461	0.0500	2.6E−05	0.0484	2.3E−05
60	3.80	135	18.02	0.0405	0.0412	3.3E−06	0.0411	2.9E−06
61	3.46	120	18.07	0.0411	0.0410	2.0E−06	0.0409	1.7E−06
62	1.60	60	17.73	0.0369	0.0432	5.8E−07	0.0432	5.6E−07
63	1.52	30	8.08	0.0408	0.0479	8.6E−05	0.0426	2.8E−05
64	3.77	150	11.76	0.0438	0.0417	5.8E−06	0.0417	5.2E−06
65	3.36	90	21.67	0.0397	0.0420	4.0E−06	0.0416	3.2E−06
66	2.60	60	18.56	0.0394	0.0420	2.0E−06	0.0418	1.9E−06
67	1.21	120	23.76	0.0340	0.0571	6.9E−06	0.0567	6.7E−06
68	2.90	30	5.96	0.0524	0.0659	7.4E−05	0.0642	5.2E−05
69	1.57	30	7.58	0.0416	0.0458	3.6E−05	0.0429	1.8E−05
70	2.35	135	12.39	0.0417	0.0398	1.4E−06	0.0398	1.2E−06
71	3.45	45	24.22	0.0373	0.0453	2.6E−06	0.0452	2.5E−06
72	1.54	135	11.92	0.0387	0.0402	5.6E−06	0.0402	4.3E−06

Table A.7
The simulated sea states and the tuning inputs and outputs of β_{44} — Case_GMT for Seed45 with 1-step tuning.

SS_n	H_s	β_W	T_p	β^*_{44}	$\bar{\beta}_{44}$	$\bar{\sigma}^2_{\beta_{44}}$	$\hat{\beta}_{44}$	$\hat{\sigma}^2_{\beta_{44}}$
1	3.97	45	22.60	0.0384	0.0700	4.0E−04	0.0637	3.8E−04
2	2.65	135	8.23	0.0499	0.0699	4.0E−04	0.0607	2.3E−04
3	1.84	105	11.10	0.0439	0.0660	3.0E−04	0.0444	5.1E−05
4	1.23	120	17.10	0.0358	0.0613	3.5E−04	0.0435	6.6E−05
5	2.33	75	23.81	0.0372	0.0606	2.7E−04	0.0424	3.0E−05
6	2.42	90	19.66	0.0391	0.0467	5.9E−05	0.0416	1.4E−05
7	1.15	30	5.79	0.0435	0.0699	4.0E−04	0.0679	4.2E−04
8	1.49	135	8.20	0.0425	0.0636	3.1E−04	0.0565	1.8E−04
9	1.35	90	6.28	0.0500	0.0668	2.9E−04	0.0651	9.9E−05
10	2.88	30	13.89	0.0392	0.0411	7.6E−05	0.0419	4.8E−05
11	3.57	45	21.80	0.0383	0.0458	2.1E−05	0.0448	1.8E−05
12	2.95	60	16.15	0.0416	0.0450	5.1E−05	0.0432	2.8E−05
13	3.97	135	24.76	0.0376	0.0531	6.5E−05	0.0481	4.2E−05
14	2.41	150	20.26	0.0353	0.0461	7.8E−05	0.0461	7.5E−05
15	2.85	60	23.82	0.0375	0.0447	9.8E−06	0.0439	8.5E−06
16	1.85	105	19.53	0.0377	0.0407	5.5E−05	0.0404	1.5E−05
17	3.93	150	10.05	0.0468	0.0507	6.4E−05	0.0535	4.6E−05
18	3.02	30	23.15	0.0355	0.0450	3.6E−05	0.0450	3.4E−05
19	2.32	150	18.69	0.0357	0.0456	2.8E−05	0.0456	2.7E−05
20	1.87	75	7.10	0.0524	0.0648	1.4E−04	0.0612	3.5E−05
21	2.53	105	17.08	0.0407	0.0421	1.1E−05	0.0413	6.2E−06
22	1.34	135	19.75	0.0346	0.0494	3.6E−05	0.0479	3.1E−05
23	1.68	105	9.74	0.0448	0.0517	4.4E−05	0.0484	3.2E−05
24	2.44	90	24.78	0.0371	0.0444	6.0E−06	0.0437	5.3E−06
25	1.73	30	21.82	0.0340	0.0509	3.4E−05	0.0509	3.2E−05
26	2.16	150	13.66	0.0375	0.0453	5.0E−05	0.0441	3.8E−05
27	3.46	30	19.46	0.0375	0.0408	9.5E−06	0.0408	9.2E−06
28	1.22	135	18.37	0.0348	0.0489	1.6E−05	0.0479	1.4E−05
29	3.77	150	15.47	0.0403	0.0392	1.5E−05	0.0394	1.2E−05
30	1.67	45	10.96	0.0401	0.0466	4.3E−05	0.0434	2.2E−05
31	3.12	30	16.42	0.0382	0.0405	7.4E−06	0.0405	6.5E−06
32	1.33	120	16.48	0.0364	0.0437	6.4E−06	0.0430	5.5E−06
33	2.80	105	5.89	0.0641	0.0686	3.6E−04	0.0764	1.2E−04
34	2.22	150	14.07	0.0374	0.0427	7.2E−06	0.0425	6.6E−06
35	3.51	45	24.80	0.0372	0.0445	2.8E−06	0.0444	2.7E−06
36	1.75	135	9.53	0.0421	0.0484	2.7E−05	0.0467	2.2E−05
37	2.37	150	14.46	0.0376	0.0420	2.8E−06	0.0419	2.6E−06
38	2.67	60	6.58	0.0582	0.0698	1.0E−04	0.0680	1.3E−04
39	1.76	45	24.35	0.0345	0.0484	1.9E−05	0.0478	1.7E−05
40	1.33	45	13.15	0.0371	0.0446	1.3E−05	0.0435	1.0E−05
41	3.18	75	5.61	0.0683	0.0749	1.8E−04	0.0749	1.7E−04
42	1.93	120	6.50	0.0530	0.0640	4.4E−05	0.0622	2.7E−05
43	3.48	75	6.49	0.0646	0.0735	2.5E−04	0.0862	1.3E−04
44	2.35	60	12.47	0.0437	0.0441	1.8E−05	0.0432	1.2E−05
45	1.28	150	8.69	0.0393	0.0565	1.4E−04	0.0511	9.6E−05
46	3.66	75	7.58	0.0604	0.0793	2.2E−04	0.0658	4.8E−05
47	3.23	60	9.73	0.0506	0.0599	1.9E−04	0.0590	6.5E−05
48	1.37	150	13.14	0.0362	0.0475	2.9E−05	0.0463	2.4E−05
49	3.57	120	6.41	0.0635	0.0781	6.4E−05	0.0729	5.4E−05
50	1.20	150	11.91	0.0365	0.0480	2.6E−05	0.0461	2.1E−05

Table A.7 (*continued*).

SS_n	H_s	β_W	T_p	β^*_{44}	$\bar{\beta}_{44}$	$\bar{\sigma}^2_{\beta_{44}}$	$\hat{\beta}_{44}$	$\hat{\sigma}^2_{\beta_{44}}$
51	1.55	60	7.95	0.0456	0.0551	3.7E−05	0.0490	2.0E−05
52	1.52	45	12.61	0.0381	0.0427	2.9E−06	0.0424	2.6E−06
53	3.77	30	19.75	0.0379	0.0401	4.3E−06	0.0401	4.1E−06
54	3.00	45	22.49	0.0374	0.0411	5.9E−06	0.0410	5.2E−06
55	1.77	120	23.59	0.0355	0.0450	7.4E−06	0.0445	6.9E−06
56	1.75	45	7.27	0.0461	0.0545	2.8E−05	0.0499	2.2E−05
57	3.95	75	15.69	0.0448	0.0660	3.4E−04	0.0497	1.1E−04
58	3.04	135	13.27	0.0431	0.0425	7.1E−06	0.0421	5.8E−06
59	2.21	60	24.30	0.0364	0.0424	4.3E−06	0.0422	4.0E−06
60	1.19	45	17.09	0.0351	0.0470	5.5E−06	0.0465	5.2E−06
61	2.33	75	21.20	0.0381	0.0408	1.7E−06	0.0407	1.4E−06
62	1.62	150	20.07	0.0342	0.0498	6.3E−06	0.0498	6.1E−06
63	1.97	150	18.11	0.0352	0.0461	1.9E−06	0.0461	1.9E−06
64	2.95	60	12.56	0.0451	0.0476	1.9E−05	0.0474	1.6E−05
65	3.17	135	11.35	0.0458	0.0485	9.0E−06	0.0484	8.6E−06
66	2.40	90	7.19	0.0562	0.0684	6.8E−05	0.0640	2.4E−05
67	1.56	105	11.18	0.0421	0.0442	7.4E−06	0.0427	5.3E−06
68	1.89	105	16.77	0.0392	0.0392	2.0E−06	0.0394	1.5E−06
69	1.42	150	12.77	0.0365	0.0456	5.3E−06	0.0452	5.0E−06
70	1.28	135	20.01	0.0345	0.0485	1.6E−06	0.0484	1.5E−06
71	2.48	30	22.41	0.0349	0.0468	3.1E−06	0.0468	3.0E−06
72	3.97	45	23.64	0.0380	0.0487	1.3E−05	0.0482	1.3E−05

Table A.8
The simulated sea states and the tuning inputs and outputs of β_{44} — Case_XCG for Seed128 with 1-step tuning.

SS_n	H_s	β_W	T_p	β^*_{44}	$\bar{\beta}_{44}$	$\bar{\sigma}^2_{\beta_{44}}$	$\hat{\beta}_{44}$	$\hat{\sigma}^2_{\beta_{44}}$
1	3.60	150	22.59	0.0366	0.0700	4.0E−04	0.0700	3.9E−04
2	1.79	30	19.40	0.0346	0.0700	4.0E−04	0.0665	3.4E−04
3	1.39	45	22.73	0.0341	0.0683	1.8E−04	0.0649	2.0E−04
4	1.12	75	15.63	0.0365	0.0673	1.7E−04	0.0437	2.8E−05
5	1.72	90	20.17	0.0372	0.0607	1.5E−04	0.0470	7.5E−05
6	2.94	150	20.40	0.0362	0.0505	4.6E−05	0.0480	3.6E−05
7	3.37	90	15.17	0.0443	0.0697	4.0E−04	0.0416	1.8E−05
8	2.80	90	15.59	0.0426	0.0483	1.8E−04	0.0408	1.4E−05
9	2.00	45	17.27	0.0372	0.0452	2.5E−05	0.0437	1.7E−05
10	1.36	105	11.12	0.0408	0.0470	1.9E−04	0.0413	1.9E−05
11	1.93	135	16.25	0.0375	0.0426	1.1E−05	0.0426	9.6E−06
12	1.33	120	15.00	0.0371	0.0431	1.2E−05	0.0422	8.6E−06
13	2.81	150	18.00	0.0369	0.0454	5.5E−06	0.0451	5.3E−06
14	1.75	75	6.48	0.0533	0.0685	3.9E−04	0.0764	3.8E−04
15	1.90	120	7.72	0.0490	0.0655	2.1E−04	0.0611	4.9E−05
16	2.55	120	8.27	0.0518	0.0613	2.2E−04	0.0605	4.3E−05
17	3.15	60	8.94	0.0523	0.0583	1.6E−04	0.0583	9.7E−05
18	3.79	60	13.38	0.0461	0.0425	3.8E−05	0.0451	2.8E−05
19	1.31	30	24.86	0.0331	0.0663	1.4E−04	0.0649	1.4E−04
20	3.12	60	11.44	0.0471	0.0475	7.2E−05	0.0466	4.3E−05
21	3.96	60	8.82	0.0555	0.0627	2.2E−04	0.0616	6.1E−05
22	2.68	150	22.73	0.0351	0.0533	2.3E−05	0.0533	2.2E−05
23	2.78	135	14.87	0.0411	0.0428	6.9E−05	0.0462	5.1E−05
24	3.23	90	22.04	0.0393	0.0452	1.0E−04	0.0411	1.9E−05
25	3.46	90	24.63	0.0386	0.0454	4.8E−05	0.0427	2.3E−05
26	1.38	105	22.24	0.0352	0.0524	9.4E−06	0.0516	8.8E−06
27	3.72	135	22.40	0.0382	0.0473	6.8E−05	0.0461	5.5E−05
28	2.72	30	17.03	0.0371	0.0438	2.2E−06	0.0437	2.1E−06
29	3.19	45	10.69	0.0469	0.0499	5.4E−05	0.0515	3.8E−05
30	1.90	135	20.10	0.0359	0.0488	2.1E−06	0.0486	2.1E−06
31	1.20	30	21.08	0.0335	0.0635	6.8E−05	0.0634	6.9E−05
32	1.49	30	9.75	0.0388	0.0538	1.8E−04	0.0422	3.3E−05
33	1.40	60	8.80	0.0430	0.0492	5.0E−05	0.0425	1.4E−05
34	2.97	105	24.73	0.0377	0.0449	3.1E−05	0.0433	2.1E−05
35	2.27	135	12.44	0.0413	0.0420	1.8E−05	0.0414	1.2E−05
36	3.95	90	13.38	0.0479	0.0560	1.6E−04	0.0443	3.9E−05
37	2.21	105	23.40	0.0371	0.0517	4.9E−05	0.0470	3.4E−05
38	1.76	45	21.29	0.0352	0.0515	2.7E−06	0.0512	2.6E−06
39	1.65	105	21.79	0.0362	0.0494	6.5E−06	0.0487	6.1E−06
40	3.53	120	5.73	0.0673	0.0704	3.8E−04	0.0773	1.4E−04
41	3.07	45	23.35	0.0372	0.0484	1.7E−05	0.0478	1.6E−05
42	1.61	120	6.32	0.0504	0.0693	1.8E−04	0.0636	7.2E−05
43	3.12	75	17.62	0.0415	0.0404	8.2E−06	0.0402	4.3E−06

(*continued on next page*)

Table A.8 (*continued*).

SS_n	H_s	β_W	T_p	β^*_{44}	$\bar{\beta}_{44}$	$\bar{\sigma}^2_{\beta_{44}}$	$\hat{\beta}_{44}$	$\hat{\sigma}^2_{\beta_{44}}$
44	3.52	30	12.51	0.0422	0.0436	1.0E−05	0.0426	7.6E−06
45	3.24	90	12.25	0.0475	0.0464	1.9E−05	0.0446	1.4E−05
46	3.25	60	5.83	0.0651	0.0755	1.3E−04	0.0697	8.2E−05
47	1.67	75	17.27	0.0380	0.0436	3.3E−06	0.0430	2.9E−06
48	1.72	60	11.88	0.0412	0.0407	5.4E−06	0.0405	3.3E−06
49	3.63	60	24.95	0.0380	0.0427	1.0E−05	0.0424	8.5E−06
50	3.61	105	17.85	0.0423	0.0410	1.3E−05	0.0406	6.5E−06
51	2.83	75	13.71	0.0443	0.0432	1.0E−05	0.0421	6.6E−06
52	1.62	150	16.24	0.0353	0.0514	2.0E−05	0.0510	1.9E−05
53	1.62	30	10.67	0.0383	0.0417	2.2E−05	0.0416	1.3E−05
54	2.31	60	18.50	0.0389	0.0448	6.6E−06	0.0438	5.7E−06
55	2.70	135	21.01	0.0375	0.0467	3.0E−06	0.0466	2.9E−06
56	3.27	60	22.06	0.0387	0.0425	5.3E−06	0.0422	4.5E−06
57	2.55	75	24.19	0.0373	0.0462	6.9E−06	0.0451	6.3E−06
58	3.06	45	20.93	0.0381	0.0454	2.3E−06	0.0453	2.2E−06
59	1.77	120	8.54	0.0461	0.0510	1.7E−05	0.0498	1.6E−05
60	3.80	135	18.02	0.0405	0.0411	3.3E−06	0.0410	2.9E−06
61	3.46	120	18.07	0.0411	0.0402	1.9E−06	0.0402	1.6E−06
62	1.60	60	17.73	0.0369	0.0446	6.4E−07	0.0445	6.1E−07
63	1.52	30	8.08	0.0408	0.0469	7.8E−05	0.0414	1.8E−05
64	3.77	150	11.76	0.0438	0.0453	6.6E−06	0.0447	6.1E−06
65	3.36	90	21.67	0.0397	0.0414	3.5E−06	0.0411	2.8E−06
66	2.60	60	18.56	0.0394	0.0433	2.2E−06	0.0429	2.1E−06
67	1.21	120	23.76	0.0340	0.0576	6.7E−06	0.0572	6.6E−06
68	2.90	30	5.96	0.0524	0.0679	8.3E−05	0.0661	6.8E−05
69	1.57	30	7.58	0.0416	0.0447	2.8E−05	0.0421	1.3E−05
70	2.35	135	12.39	0.0417	0.0417	1.6E−06	0.0415	1.4E−06
71	3.45	45	24.22	0.0373	0.0458	2.7E−06	0.0457	2.6E−06
72	1.54	135	11.92	0.0387	0.0399	5.4E−06	0.0399	4.1E−06

Table A.9
The simulated sea states and the tuning inputs and outputs of β_{44} — Case_GMT for Seed45 with 2-step tuning.

SS_n	H_s	β_W	T_p	β^*_{44}	$\bar{\beta}_{44}$	$\bar{\sigma}^2_{\beta_{44}}$	$\hat{\beta}_{44}$	$\hat{\sigma}^2_{\beta_{44}}$
1	3.97	45	22.60	0.0384	0.0700	4.0E−04	0.0624	3.8E−04
2	2.65	135	8.23	0.0499	0.0699	4.0E−04	0.0593	2.1E−04
3	1.84	105	11.10	0.0439	0.0653	3.0E−04	0.0435	3.5E−05
4	1.23	120	17.10	0.0358	0.0607	3.5E−04	0.0423	3.9E−05
5	2.33	75	23.81	0.0372	0.0597	2.7E−04	0.0420	2.6E−05
6	2.42	90	19.66	0.0391	0.0460	5.6E−05	0.0415	1.3E−05
7	1.15	30	5.79	0.0435	0.0699	4.0E−04	0.0726	4.3E−04
8	1.49	135	8.20	0.0425	0.0633	3.1E−04	0.0509	1.6E−04
9	1.35	90	6.28	0.0500	0.0661	2.8E−04	0.0644	8.3E−05
10	2.88	30	13.89	0.0392	0.0392	6.4E−05	0.0405	3.8E−05
11	3.57	45	21.80	0.0383	0.0454	2.1E−05	0.0445	1.7E−05
12	2.95	60	16.15	0.0416	0.0448	4.9E−05	0.0427	2.5E−05
13	3.97	135	24.76	0.0376	0.0527	6.4E−05	0.0477	4.0E−05
14	2.41	150	20.26	0.0353	0.0445	6.3E−05	0.0445	6.1E−05
15	2.85	60	23.82	0.0375	0.0444	9.2E−06	0.0436	7.9E−06
16	1.85	105	19.53	0.0377	0.0401	5.2E−05	0.0402	1.4E−05
17	3.93	150	10.05	0.0468	0.0496	5.3E−05	0.0521	4.2E−05
18	3.02	30	23.15	0.0355	0.0443	3.3E−05	0.0443	3.2E−05
19	2.32	150	18.69	0.0357	0.0439	2.0E−05	0.0439	1.9E−05
20	1.87	75	7.10	0.0524	0.0633	1.3E−04	0.0606	3.1E−05
21	2.53	105	17.08	0.0407	0.0417	1.0E−05	0.0409	5.1E−06
22	1.34	135	19.75	0.0346	0.0474	3.0E−05	0.0463	2.6E−05
23	1.68	105	9.74	0.0448	0.0492	3.9E−05	0.0462	2.5E−05
24	2.44	90	24.78	0.0371	0.0442	5.6E−06	0.0434	4.9E−06
25	1.73	30	21.82	0.0340	0.0492	3.0E−05	0.0492	2.9E−05
26	2.16	150	13.66	0.0375	0.0429	4.4E−05	0.0423	3.2E−05
27	3.46	30	19.46	0.0375	0.0404	8.7E−06	0.0404	8.4E−06
28	1.22	135	18.37	0.0348	0.0470	1.4E−05	0.0462	1.2E−05
29	3.77	150	15.47	0.0403	0.0388	1.4E−05	0.0390	1.1E−05
30	1.67	45	10.96	0.0401	0.0438	3.8E−05	0.0419	1.9E−05
31	3.12	30	16.42	0.0382	0.0397	6.5E−06	0.0398	5.7E−06
32	1.33	120	16.48	0.0364	0.0422	5.3E−06	0.0418	4.4E−06
33	2.80	105	5.89	0.0641	0.0690	3.6E−04	0.0774	7.9E−05
34	2.22	150	14.07	0.0374	0.0413	6.2E−06	0.0412	5.6E−06
35	3.51	45	24.80	0.0372	0.0442	2.6E−06	0.0441	2.5E−06
36	1.75	135	9.53	0.0421	0.0457	2.3E−05	0.0441	1.7E−05
37	2.37	150	14.46	0.0376	0.0407	2.3E−06	0.0407	2.2E−06
38	2.67	60	6.58	0.0582	0.0709	9.1E−05	0.0704	1.2E−04

Table A.9 (*continued*).

SS_n	H_s	β_W	T_p	β^*_{44}	$\bar{\beta}_{44}$	$\bar{\sigma}^2_{\beta_{44}}$	$\hat{\beta}_{44}$	$\hat{\sigma}^2_{\beta_{44}}$
39	1.76	45	24.35	0.0345	0.0471	1.7E−05	0.0465	1.6E−05
40	1.33	45	13.15	0.0371	0.0432	1.2E−05	0.0424	8.8E−06
41	3.18	75	5.61	0.0683	0.0758	1.5E−04	0.0758	1.5E−04
42	1.93	120	6.50	0.0530	0.0637	4.0E−05	0.0620	2.3E−05
43	3.48	75	6.49	0.0646	0.0743	2.5E−04	0.0866	1.2E−04
44	2.35	60	12.47	0.0437	0.0434	1.6E−05	0.0417	7.8E−06
45	1.28	150	8.69	0.0393	0.0541	1.3E−04	0.0457	5.8E−05
46	3.66	75	7.58	0.0604	0.0797	2.1E−04	0.0620	1.8E−05
47	3.23	60	9.73	0.0506	0.0571	1.8E−04	0.0569	6.7E−05
48	1.37	150	13.14	0.0362	0.0459	2.6E−05	0.0449	2.2E−05
49	3.57	120	6.41	0.0635	0.0783	5.9E−05	0.0715	4.4E−05
50	1.20	150	11.91	0.0365	0.0460	2.3E−05	0.0446	1.8E−05
51	1.55	60	7.95	0.0456	0.0518	3.4E−05	0.0473	1.8E−05
52	1.52	45	12.61	0.0381	0.0413	2.5E−06	0.0411	2.2E−06
53	3.77	30	19.75	0.0379	0.0399	3.9E−06	0.0399	3.8E−06
54	3.00	45	22.49	0.0374	0.0411	5.5E−06	0.0410	4.9E−06
55	1.77	120	23.59	0.0355	0.0443	6.9E−06	0.0439	6.3E−06
56	1.75	45	7.27	0.0461	0.0524	2.6E−05	0.0476	1.7E−05
57	3.95	75	15.69	0.0448	0.0654	3.4E−04	0.0462	7.1E−05
58	3.04	135	13.27	0.0431	0.0413	5.5E−06	0.0411	4.3E−06
59	2.21	60	24.30	0.0364	0.0423	4.1E−06	0.0421	3.8E−06
60	1.19	45	17.09	0.0351	0.0454	4.8E−06	0.0450	4.6E−06
61	2.33	75	21.20	0.0381	0.0407	1.6E−06	0.0406	1.3E−06
62	1.62	150	20.07	0.0342	0.0481	5.7E−06	0.0481	5.5E−06
63	1.97	150	18.11	0.0352	0.0445	1.6E−06	0.0445	1.6E−06
64	2.95	60	12.56	0.0451	0.0462	1.8E−05	0.0457	1.5E−05
65	3.17	135	11.35	0.0458	0.0469	7.9E−06	0.0463	7.6E−06
66	2.40	90	7.19	0.0562	0.0685	6.4E−05	0.0640	2.1E−05
67	1.56	105	11.18	0.0421	0.0427	6.3E−06	0.0416	4.0E−06
68	1.89	105	16.77	0.0392	0.0389	1.8E−06	0.0391	1.4E−06
69	1.42	150	12.77	0.0365	0.0443	4.7E−06	0.0439	4.4E−06
70	1.28	135	20.01	0.0345	0.0469	1.4E−06	0.0468	1.4E−06
71	2.48	30	22.41	0.0349	0.0455	2.8E−06	0.0455	2.7E−06
72	3.97	45	23.64	0.0380	0.0480	1.3E−05	0.0475	1.2E−05

Table A.10
The simulated sea states and the tuning inputs and outputs of β_{44} — Case_XCG for Seed128 with 2-step tuning.

SS_n	H_s	β_W	T_p	β^*_{44}	$\bar{\beta}_{44}$	$\bar{\sigma}^2_{\beta_{44}}$	$\hat{\beta}_{44}$	$\hat{\sigma}^2_{\beta_{44}}$
1	3.60	150	22.59	0.0366	0.0700	4.0E−04	0.0700	3.9E−04
2	1.79	30	19.40	0.0346	0.0700	4.0E−04	0.0665	3.3E−04
3	1.39	45	22.73	0.0341	0.0682	1.8E−04	0.0638	1.9E−04
4	1.12	75	15.63	0.0365	0.0670	1.7E−04	0.0431	2.1E−05
5	1.72	90	20.17	0.0372	0.0601	1.5E−04	0.0456	5.6E−05
6	2.94	150	20.40	0.0362	0.0486	4.0E−05	0.0465	3.1E−05
7	3.37	90	15.17	0.0443	0.0696	4.0E−04	0.0414	1.6E−05
8	2.80	90	15.59	0.0426	0.0477	1.8E−04	0.0407	1.2E−05
9	2.00	45	17.27	0.0372	0.0436	2.2E−05	0.0425	1.4E−05
10	1.36	105	11.12	0.0408	0.0463	1.8E−04	0.0411	1.7E−05
11	1.93	135	16.25	0.0375	0.0413	9.4E−06	0.0414	7.7E−06
12	1.33	120	15.00	0.0371	0.0422	1.0E−05	0.0416	7.0E−06
13	2.81	150	18.00	0.0369	0.0441	4.7E−06	0.0438	4.4E−06
14	1.75	75	6.48	0.0533	0.0685	3.9E−04	0.0748	2.9E−04
15	1.90	120	7.72	0.0490	0.0652	2.0E−04	0.0611	4.1E−05
16	2.55	120	8.27	0.0518	0.0612	2.2E−04	0.0605	3.6E−05
17	3.15	60	8.94	0.0523	0.0583	1.6E−04	0.0579	9.1E−05
18	3.79	60	13.38	0.0461	0.0421	3.6E−05	0.0448	2.5E−05
19	1.31	30	24.86	0.0331	0.0660	1.4E−04	0.0643	1.4E−04
20	3.12	60	11.44	0.0471	0.0474	7.0E−05	0.0455	3.8E−05
21	3.96	60	8.82	0.0555	0.0625	2.2E−04	0.0611	4.7E−05
22	2.68	150	22.73	0.0351	0.0519	2.2E−05	0.0519	2.1E−05
23	2.78	135	14.87	0.0411	0.0415	6.6E−05	0.0451	4.7E−05
24	3.23	90	22.04	0.0393	0.0452	1.0E−04	0.0410	1.8E−05
25	3.46	90	24.63	0.0386	0.0452	4.7E−05	0.0424	2.1E−05
26	1.38	105	22.24	0.0352	0.0510	8.8E−06	0.0502	8.2E−06
27	3.72	135	22.40	0.0382	0.0472	6.6E−05	0.0458	5.1E−05
28	2.72	30	17.03	0.0371	0.0426	1.9E−06	0.0425	1.8E−06
29	3.19	45	10.69	0.0469	0.0492	5.1E−05	0.0505	3.4E−05
30	1.90	135	20.10	0.0359	0.0474	2.0E−06	0.0473	1.9E−06
31	1.20	30	21.08	0.0335	0.0631	6.6E−05	0.0632	6.7E−05
32	1.49	30	9.75	0.0388	0.0539	1.8E−04	0.0423	3.0E−05

(*continued on next page*)

Table A.10 (*continued*).

SS_n	H_s	β_W	T_p	β^*_{44}	$\bar{\beta}_{44}$	$\bar{\sigma}^2_{\beta_{44}}$	$\hat{\beta}_{44}$	$\hat{\sigma}^2_{\beta_{44}}$
33	1.40	60	8.80	0.0430	0.0491	4.6E−05	0.0423	1.2E−05
34	2.97	105	24.73	0.0377	0.0448	2.9E−05	0.0431	1.9E−05
35	2.27	135	12.44	0.0413	0.0413	1.6E−05	0.0409	1.0E−05
36	3.95	90	13.38	0.0479	0.0556	1.6E−04	0.0437	3.2E−05
37	2.21	105	23.40	0.0371	0.0508	4.6E−05	0.0460	2.8E−05
38	1.76	45	21.29	0.0352	0.0502	2.6E−06	0.0499	2.4E−06
39	1.65	105	21.79	0.0362	0.0479	5.8E−06	0.0472	5.5E−06
40	3.53	120	5.73	0.0673	0.0705	3.8E−04	0.0770	1.1E−04
41	3.07	45	23.35	0.0372	0.0474	1.5E−05	0.0468	1.4E−05
42	1.61	120	6.32	0.0504	0.0691	1.7E−04	0.0625	5.8E−05
43	3.12	75	17.62	0.0415	0.0403	7.7E−06	0.0402	4.0E−06
44	3.52	30	12.51	0.0422	0.0428	9.2E−06	0.0420	6.6E−06
45	3.24	90	12.25	0.0475	0.0460	1.8E−05	0.0442	1.3E−05
46	3.25	60	5.83	0.0651	0.0755	1.2E−04	0.0691	6.8E−05
47	1.67	75	17.27	0.0380	0.0423	2.9E−06	0.0418	2.4E−06
48	1.72	60	11.88	0.0412	0.0403	4.8E−06	0.0402	2.9E−06
49	3.63	60	24.95	0.0380	0.0426	9.4E−06	0.0422	7.8E−06
50	3.61	105	17.85	0.0423	0.0408	1.2E−05	0.0404	6.0E−06
51	2.83	75	13.71	0.0443	0.0427	9.4E−06	0.0417	5.8E−06
52	1.62	150	16.24	0.0353	0.0510	1.9E−05	0.0506	1.8E−05
53	1.62	30	10.67	0.0383	0.0418	2.0E−05	0.0417	1.2E−05
54	2.31	60	18.50	0.0389	0.0436	6.1E−06	0.0428	4.9E−06
55	2.70	135	21.01	0.0375	0.0455	2.7E−06	0.0453	2.6E−06
56	3.27	60	22.06	0.0387	0.0424	4.9E−06	0.0420	4.2E−06
57	2.55	75	24.19	0.0373	0.0456	6.4E−06	0.0446	5.7E−06
58	3.06	45	20.93	0.0381	0.0445	2.1E−06	0.0444	2.0E−06
59	1.77	120	8.54	0.0461	0.0510	1.6E−05	0.0496	1.4E−05
60	3.80	135	18.02	0.0405	0.0409	3.1E−06	0.0408	2.7E−06
61	3.46	120	18.07	0.0411	0.0402	1.7E−06	0.0402	1.5E−06
62	1.60	60	17.73	0.0369	0.0433	5.5E−07	0.0433	5.3E−07
63	1.52	30	8.08	0.0408	0.0462	7.5E−05	0.0411	1.7E−05
64	3.77	150	11.76	0.0438	0.0447	6.0E−06	0.0440	5.4E−06
65	3.36	90	21.67	0.0397	0.0412	3.3E−06	0.0410	2.5E−06
66	2.60	60	18.56	0.0394	0.0426	2.1E−06	0.0422	1.9E−06
67	1.21	120	23.76	0.0340	0.0565	6.5E−06	0.0561	6.2E−06
68	2.90	30	5.96	0.0524	0.0670	7.3E−05	0.0650	5.5E−05
69	1.57	30	7.58	0.0416	0.0441	2.6E−05	0.0419	1.2E−05
70	2.35	135	12.39	0.0417	0.0412	1.4E−06	0.0410	1.2E−06
71	3.45	45	24.22	0.0373	0.0452	2.5E−06	0.0451	2.4E−06
72	1.54	135	11.92	0.0387	0.0397	4.9E−06	0.0398	3.8E−06

References

Bitner-Gregersen, E.M., Hagen, Ø., 1990. Uncertainties in data for the offshore environment. Struct. Saf. 7 (1), 11–34. http://dx.doi.org/10.1016/0167-4730(90)90010-M.

DNV GL, 2018. Wasim user manual. Technical Report.

DNVGL-ST-N001, 2016. Marine operations and marine warranty.

Erickson, C.B., Ankenman, B.E., Sanchez, S.M., 2018. Comparison of Gaussian process modeling software. European Journal of Operational Research (ISSN: 0377-2217) 266 (1), 179–192. http://dx.doi.org/10.1016/j.ejor.2017.10.002.

Falzarano, J., Somayajula, A., Seah, R., 2015. An overview of the prediction methods for roll damping of ships. Ocean Syst. Eng. 5 (2), 55–76.

Han, X., Leira, B.J., Sævik, S., 2021a. Vessel hydrodynamic model tuning by discrete Bayesian updating using simulated onboard sensor data. Ocean Eng. 220, http://dx.doi.org/10.1016/j.oceaneng.2020.108407, URL: https://www.sciencedirect.com/science/article/pii/S0029801820313147.

Han, X., Leira, B.J., Sævik, S., Ren, Z., 2021b. Onboard tuning of vessel seakeeping model parameters and sea state characteristics. Mar. Struct. 78, http://dx.doi.org/10.1016/j.marstruc.2021.102998.

Han, X., Ren, Z., Leira, B.J., Sævik, S., 2021c. Adaptive identification of lowpass filter cutoff frequency for online vessel model tuning. Ocean Eng. Revision under review.

Han, X., Sævik, S., Leira, B.J., 2020. A sensitivity study of vessel hydrodynamic model parameters. In: Proceedings of the ASME 2020 39th International Conference on Ocean, Offshore and Arctic Engineering, Vol. 1. Virtual, Online.

Himeno, Y., 1981. Prediction of ship roll damping - state of the art. Technical Report, The University of Michigan, College of Engineering, Department of Naval Architecture and Marine Engineering, USA.

Ikeda, Y., Himeno, Y., Tanaka, N., 1978a. On eddy making component of roll damping force on naked hull. Technical Report 00403, Osaka Prefecture University.

Ikeda, Y., Himeno, Y., Tanaka, N., 1978b. Components of roll damping of ship at forward speed. Technical Report 00404, Osaka Prefecture University.

Ikeda, Y., Himeno, Y., Tanaka, N., 1978c. A prediction method for ship roll damping. Technical Report 00405, Osaka Prefecture University.

Ikeda, Y., Komatsu, K., Tanaka, N., 1979. On roll damping force of ship-effects of hull surface pressure created by bilge keels. Technical Report 00402, Osaka Prefecture University.

Irkal, M.A.R., Nallayarasu, S., Bhattacharyya, S.K., 2016. CFD approach to roll damping of ship with bilge keel with experimental validation. Appl. Ocean Res. 55, 1–17.

ITTC, 2011. Recommended procedures and guidelines: Numerical estimation of roll damping. Technical Report, International Towing Tank Conference.

Kaplan, P., 1966. Lecture notes on nonlinear theory of ship roll motion in a random seaway.

Kring, D.C., 1994. Time domain ship motions by a three-dimensional Rankine panel method (Ph.D. thesis). Massachusetts Institute of Technology.

Labbe, R., 2018. Kalman and Bayesian filters in Python. https://github.com/rlabbe/Kalman-and-Bayesian-Filters-in-Python,

Larsen, C.M., Lian, W., Bachynski, E.E., Kristiansen, T., Myrhaug, D., 2019. Lecture notes in TMR4182 marine dynamics.

Neumann-Brosig, M., Marco, A., Schwarzmann, D., Trimpe, S., 2020. Data-efficient autotuning with Bayesian optimization: An industrial control study. IEEE Trans. Control Syst. Technol. 28 (3), 730–740.

Pedregosa, F., Varoquaux, G., Gramfort, A., Michel, V., Thirion, B., Grisel, O., Blondel, M., Prettenhofer, P., Weiss, R., Dubourg, V., Vanderplas, J., Passos, A., Cournapeau, D., Brucher, M., Perrot, M., Duchesnay, E., 2011. Scikit-learn: Machine learning in python. J. Mach. Learn. Res. 12, 2825–2830.

Qiu, W., Junior, J.S., Lee, D., Lie, H., Magarovskii, V., Mikami, T., Rousset, J.-M., Sphaier, S., Tao, L., Wang, X., 2014. Uncertainties related to predictions of loads and responses for ocean and offshore structures. Ocean Eng. 86, 58–67.

Rasmussen, C.E., Williams, C.K.I., 2006. Gaussian processes for machine learning. The MIT Press, ISBN: 026218253X, URL: https://www.GaussianProcess.org/gpml.

Scheick, J.T., 1997. Linear algebra with applications, Vol. 81. McGraw-Hill New York.

Shepard, D., 1968. A two-dimensional interpolation function for irregularly-spaced data. In: Proceedings of the 1968 23rd ACM National Conference. In: ACM '68, Association for Computing Machinery, New York, NY, USA, pp. 517–524. http://dx.doi.org/10.1145/800186.810616.

Söder, C.-J., Rosén, A., 2015. A framework for holistic roll damping prediction. In: International Ship Stability Workshop.

Söder, C.-J., Rosén, A., Huss, M., 2017. Ikeda revisited. J. Mar. Sci. Technol..